ATOMISTIC SIMULATION OF VACANCIES IN URANIUM-ZIRCONIUM ALLOYS

A Thesis
Presented to
The Academic Faculty

by

David Evan Carroll

In Partial Fulfillment
of the Requirements for the Degree
Masters of Science in Nuclear Engineering

Georgia Institute of Technology

December 2017

ATOMISTIC SIMULATION OF VACANCIES IN URANIUM-ZIRCONIUM ALLOYS

Approved by:

Dr. Chaitanya S. Deo, Advisor
School of Mechanical Engineering
Georgia Institute of Technology

Dr. Weston M. Stacey, Jr.
School of Mechanical Engineering
Georgia Institute of Technology

Dr. Hamid Garmestani
School of Materials Science and Engineering
Georgia Institute of Technology

Date Approved: 12/5/2017

ACKNOWLEDGEMENTS

TABLE OF CONTENTS

LIST OF TABLES

LIST OF FIGURES

SUMMARY

Metallic alloy fuels were often used in the infancy of nuclear power, but since the industry began focusing on oxide fuels, there hasn't been a lot of research done on metallic alloy fuels using current research capabilities. In this thesis, uranium-zirconium alloy has been selected for closer examination as zirconium is one of the cheapest of the potential alloying metals, such as molybdenum and niobium. The work will look at the vacancy formation energy of pure uranium, then alloys containing 10%, 20%, and 30% zirconium by atomic percent at temperatures ranging from 100 K to 1400 K, going in steps of 100 K. The simulations will be run using LAMMPS with a MEAM interatomic potential. It also analyzes the results and structure of these simulations using Wigner-Seitz Defect Analysis, Short Range Order Parameter, Common Neighbor Analysis, and the Radial Distribution Function.

The results show that the interatomic potential used gives accurate vacancy formation energies for pure uranium, 10% zirconium, and 20% zirconium, usually around $1 - 2$ eV. The structure for these metals also maintains the BCC phase. 30% zirconium, however, tends to give negative vacancy formation energies and has difficulty maintaining its phase, due to the creation of vacancy-interstitial pairs. In the end, the U-20Zr alloy is recommended for use in advanced reactors due to wanting as much of zirconium's thermal properties as possible while still keeping the structure intact.

Chapter 1: Introduction

As new nuclear reactors are being considered, such as fast reactors and advanced thermal reactors, new designs for key components are being considered. In America's current reactor fleet, uranium oxides are often used as they have a much higher melting point than other potential fuels, and are also inflammable, since the fuel is already in an oxidized state. However, for fast reactors, several different fuel types are being considered, chief among them being metallic alloys.

Metallic alloys were used in early experimental nuclear reactors due to their high fissile density, compatibility with the sodium coolant, and low smear density which lead to a much higher fuel burnup. Many of the first reactors used in the nuclear program's infancy utilized metallic fuels; in the U.S., the EBR-I, EBR-II, and FERMI-I used metallic alloys, as well as the DFR in the U.K. Specifically, the Integral Fast Reactor in the U.S. used U-Pu-Zr alloys and was the first program to put together a vast database on the metallic alloy fuel's performance. Mark-I, or first generation, fuel used unalloyed, highly enriched uranium metal. In EBR-I, Mk-II fuels were composed of centrifugally cast U-Zr alloy, while Mk-III fuels coextruded Mk-II fuels with a layer of Zircaloy-2 cladding. After the EBR-I, the EBR-II irradiated over 30,000 Mk-II fuel driver rods, 13,000 Mk-III/IIIA/IV driver fuel rods, and over 600 U-Pu-Zr fuel rods. So, the U-Zr alloy has long been important in nuclear fuel development and will continue to be important as advanced reactors are developed, as thermal reactors with oxide fuels have only been used in the past.

Metallic Fuel Advantages

Metallic alloy fuels are being looked at as primary fuels in advanced reactor designs currently being developed due to several traits that would help them perform better than the oxide fuels being used in the nuclear industry's current fleet of reactors. First, metallic fuels can have a higher burn-up potential due to their ability to possibly have a higher fissile atom density. Since there is more burn-up potential in the fuel, the operation time between refueling will be longer, allows smaller reactor designs with high power density, and allows more plutonium to be bred during operation time.

Advanced reactors, especially fast neutron reactors, will be operating at much higher temperatures than thermal reactors currently being operated. Metallic fuels have the thermodynamic properties required to better handle the higher temperatures, specifically a better thermal conductivity, allowing much more efficient cooling and reducing cladding and fuel temperatures.

Most of the metallic fuels will be in the BCC phase during reactor operating temperatures, leading to much more isotropic neutron cross sections. This is particularly beneficial for smaller reactors as it also allows a higher power density.

Another metallic fuel advantage is that plutonium does not have to be separated from the fuel during reprocessing. Plutonium has a very high potential to be used in nuclear devices, so proliferation experts would prefer a fuel that can be reprocessed without separating out the plutonium.

The last advantage worth mentioning is that metallic fuels have some passive safety features during core off-normal events that oxide fuels clearly do not. During a loss-of-flow event, fission gases and thermal expansion will cause the fuel to expand and swell to the

cladding, where the fuel at the interface will transform to the molten phase, reducing reactivity in the reactor and helping to prevent the core from going supercritical.

Metallic Fuel Disadvantages

However, as with any engineering solution, there are downsides to go with the upsides. Fuel swelling, fission gas release, fuel redistribution, and cladding and coolant interactions are all potential problems that need to be addressed before utilizing the metallic fuels in commercial reactors.

Fuel swelling is when the fuel's volume increases while its general shape remains the same, where as irradiation growth causes the fuel's shape to change while the volume remains the same. Both of these occur as the fuel is irradiated during reactor operation. When operation first begins, the metallic fuel swells drastically due to fission gas bubbles; once these bubbles become interconnected and create a pathway for them to escape through, the swelling slows and is mostly caused by fission products taking spots in the fuel's lattice. These fission products also bring about a decrease in thermal conductivity, as the fission products tend to have a lower thermal conductivity than the metals they are replacing. In addition, large irregular shaped cavities are caused by grain boundary tearing at the fuel edges. Both irradiation growth and grain boundary tearing can cause reactivity loss in the reactor (Pahl 1990).

The fuel cladding mechanical interaction (FCMI) is another downside that occurs as the fuel is irradiated. The fission gas pressure can cause irradiation/thermal creep until eventually the cladding undergoes a stress-rupture (Pahl 1990; Pahl 1992). Until the 1960's, when a technical breakthrough at Argonne National Lab changed things, the FCMI put a limit on the burn-up of metallic fuels. With the newly decreased FCMI, the burn-up potential of metallic fuels was finally achieved (Ogata 1996; Walters 1984). By reducing the smear density by approximately

75%, the fuel has room to swell inside the cladding, so the fission gas will connect enough to create an escape path before the stress-rupture occurs.

There is also the fuel cladding chemical interaction (FCCI), which can cause creep rupture at high burn-ups. Another result of FCCI is fuel elements such as plutonium, uranium, and fission products can diffuse into the cladding, leading to cladding wall thinning, a brittle cladding layer, and a lowered melting point due to a eutectic composition in the fuel (Pahl 1990; Hayes 2009; Ogata 1997).

Experiments have also shown that uranium and zirconium undergo redistribution when the uranium-zirconium alloys undergo irradiation, as in a nuclear reactor. However, experimentally, this interdiffusional restructuring only slightly changes the mechanical and neutronic properties of the fuel, and makes no significant change to the overall fuel lifetime, despite a lowered solidus temperature in some fuel regions (Pahl 1990; Kim 2004).
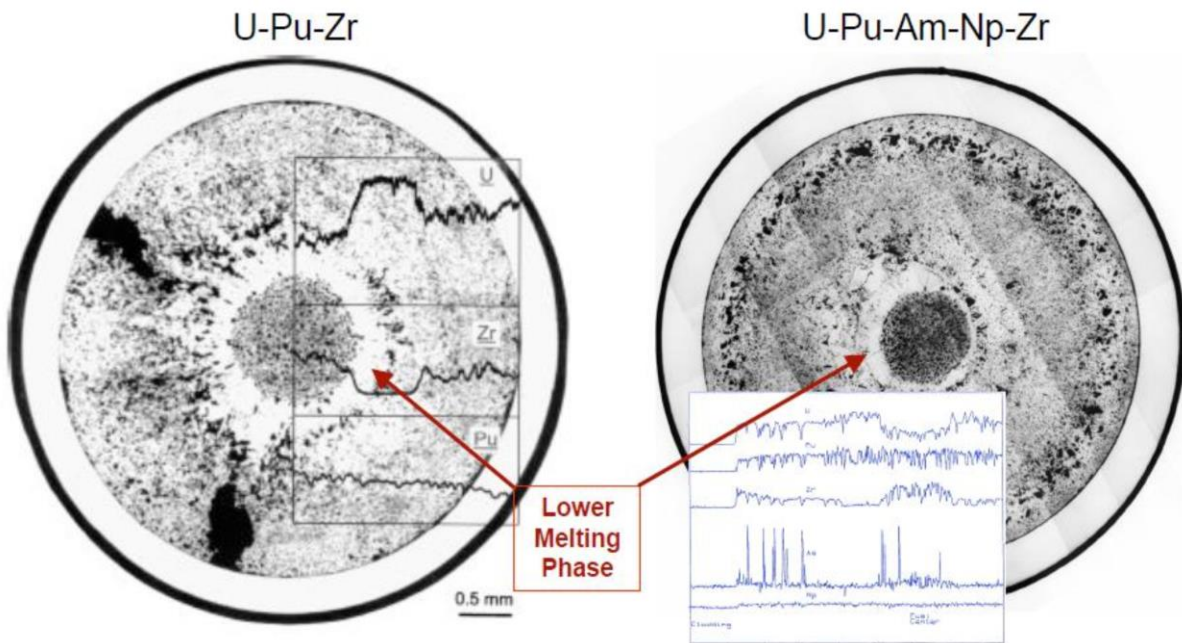
Figure 1: Post-irradiation Optical Metallography and Measured Constituent Redistributions (Kim 2004; Hofman 1996)

Another potential downside is the lower melting point of metallic alloy fuels compared to oxide fuels. Uranium in particular has a low melting point, however, by alloying to metals that are also in BCC phase at high temperatures, the melting point can be increased. So far, zirconium, molybdenum, and niobium are the alloying metals that have been studied most. One of the positives of nuclear metallic fuel, the alloy's higher thermal conductivity, could negate this negative to some degree. Since the thermal conductivity is higher, the thermal flux will be higher, allowing a lower temperature gradient and high power density while still remaining below the fuel's melting point. In addition, the lower melting point is not necessarily a total negative. In the event of a loss of cooling, the low melting point will allow the fuel to go into the molten phase earlier, reducing reactor reactivity. This is a passive safety feature of the metallic fuel.

Swelling has also been considered a potential benefit, in certain off-normal situations. The interconnected porosity of swollen metallic fuel and the low melting point during a transient event allows for the fuel's thermal expansion during temperature-induced phase transitions. This transformation prevents the cladding from being stressed by the fuel and allows the fuel to flow onto itself in the open porosity (Ondracek 1973).

There is still a lot that needs to be discovered about metallic fuels before implementation in advanced reactor designs and a lot of that information will be discovered using computational simulations. Unfortunately, a lot of the necessary tools for computational simulation of metallic fuels are not complete. Computational simulation gives the ability to see what is happening at much smaller sizes and timescales than is possible using experimentation and will also allow predictions to be made about metallic fuel properties under a variety of conditions that are not necessarily possible to make experimentally. Experimentation at higher temperatures is also

difficult due to severe thermal scatter. By using experimentation and computational simulation together, it will be possible to plan the operation and design of a reactor, as well as optimizing fabrication and processing of fuels.

Uranium (U)

Uranium is an actinide exhibiting delocalized f-electrons, and therefore has three solid allotropes: α (face-centered orthorhombic), β (body-centered tetragonal), and γ (body-centered cubic). The α state is uranium's base level allotrope but transforms into the β around 935 K, while β becomes γ at approximately 1045 K. The γ allotrope is the most interesting for advanced reactor designs as most advanced reactors operate at very high temperatures. The α, β, and γ crystal structures are shown below.
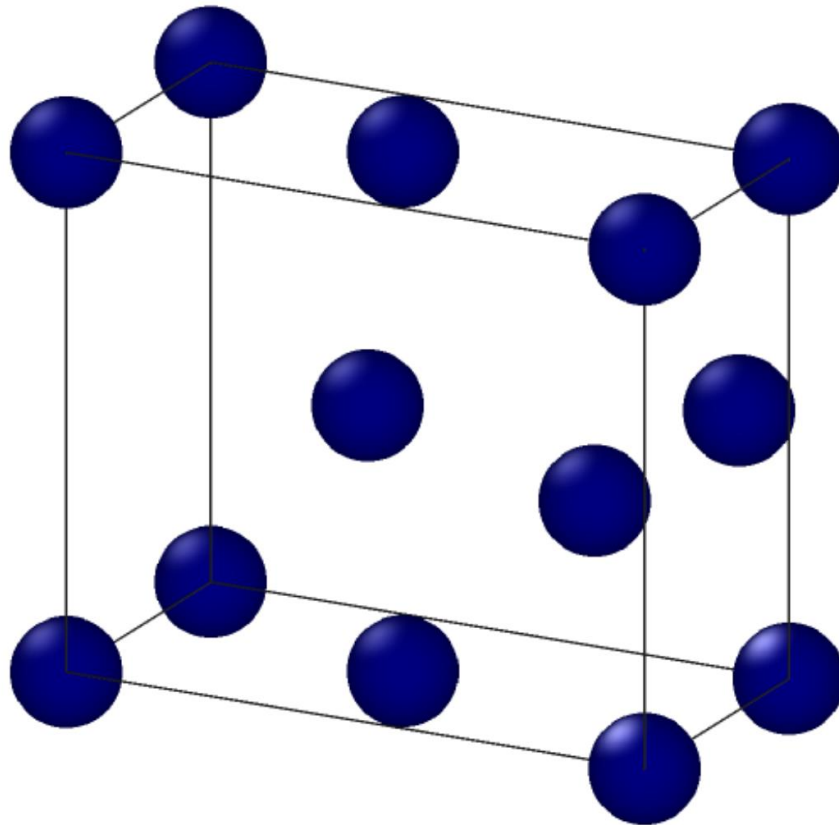
Figure 2: The Unit Cell of the α-U Crystal Structure
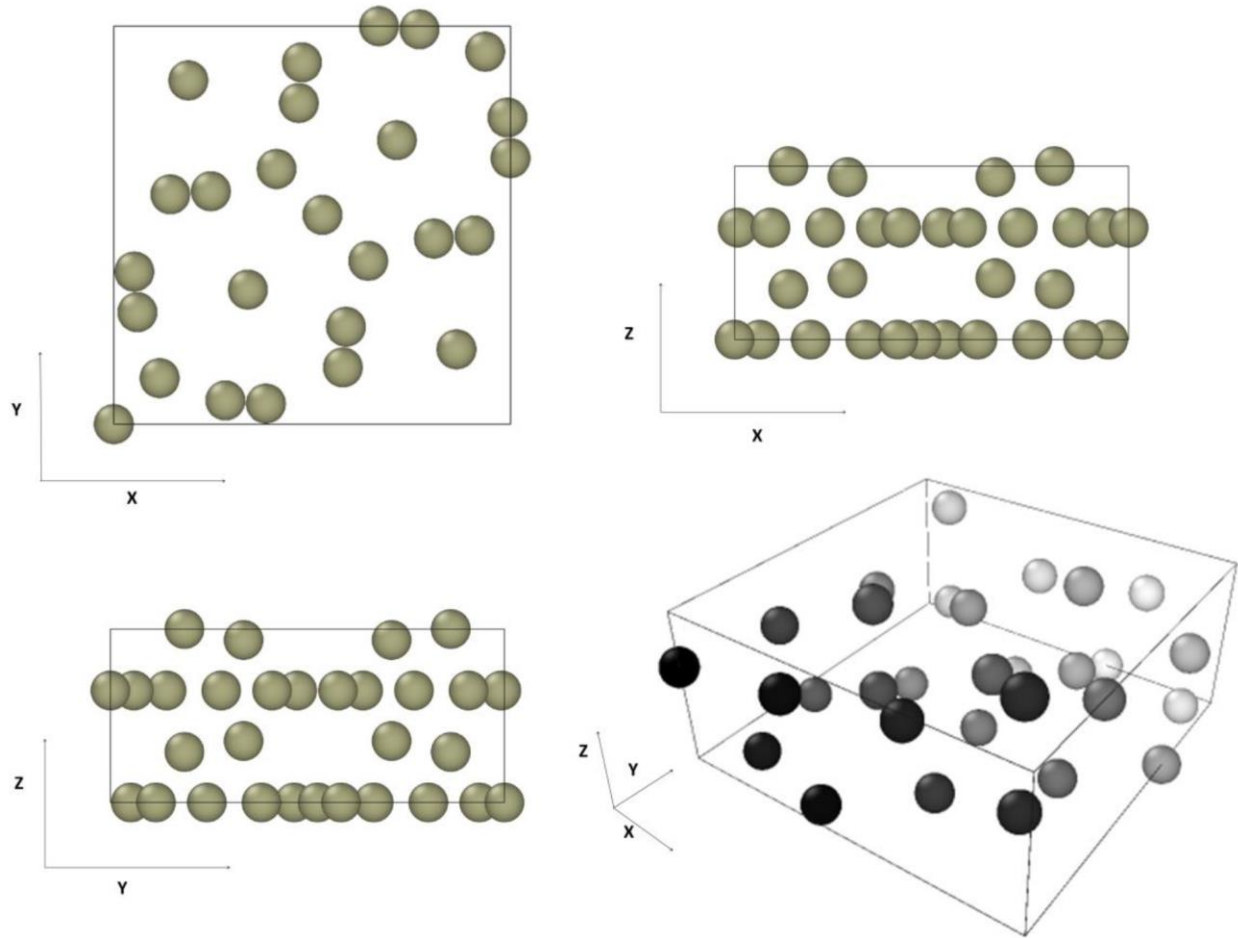
Figure 3: The β-U Crystal Structure (Beeler 2012a)
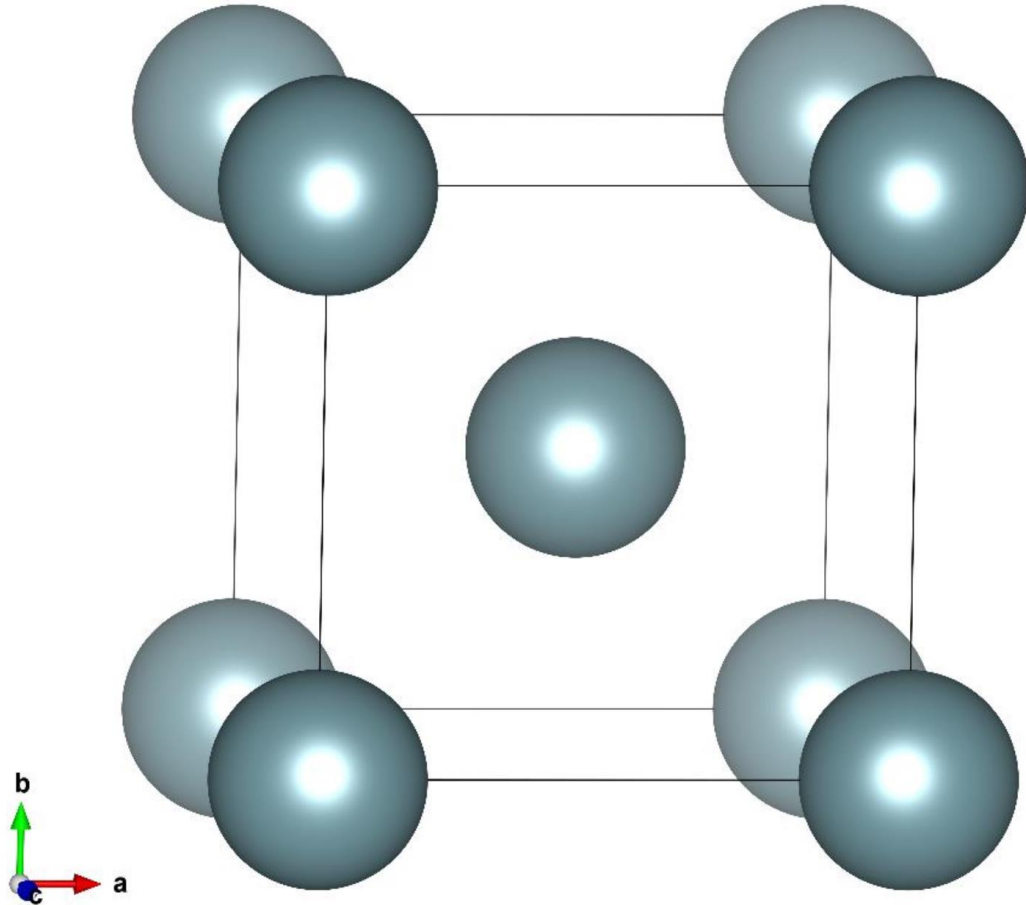
Figure 4: The γ-U Crystal Structure

Uranium's vacancy formation energies in the BCC state have been calculated in several previous studies, as shown in Table 1 below. Since then, a previous study done by Moore has found a vacancy formation energy of 1.34 eV for the uranium at 0 K.

Table 1: Vacancy Formation Energies of γ-U

E^v_{form} (PBE)	1.384 eV
E^v_{form} (PW91)	1.323 eV
E^v_{form} (Xiang) [14]	1.08 eV
E^v_{form} (Matter) [15]	1.2 ± 0.25 eV

Zirconium (Zr)

       Zirconium is a transition metal and has two solid phases. At low temperatures, it is in the α (hexagonally closed packed) phase, while starting at 863° C, it transitions to the β (body centered cubic) phase. Zirconium also has a very high melting point of 1855° C, or 2128 K. Because of the fact that both uranium and zirconium are in the bcc phase at high temperatures, zirconium is a strong candidate for alloying with uranium. In addition, the high melting point raises the melting point of uranium once the two are alloyed. In the same study done by Moore cited above, the vacancy formation energy of β zirconium was found to be 2.1 eV. Another study looking at vacancy formation energy for β zirconium at 1200 K found a value of 2.00 eV (Mendelev 2007).
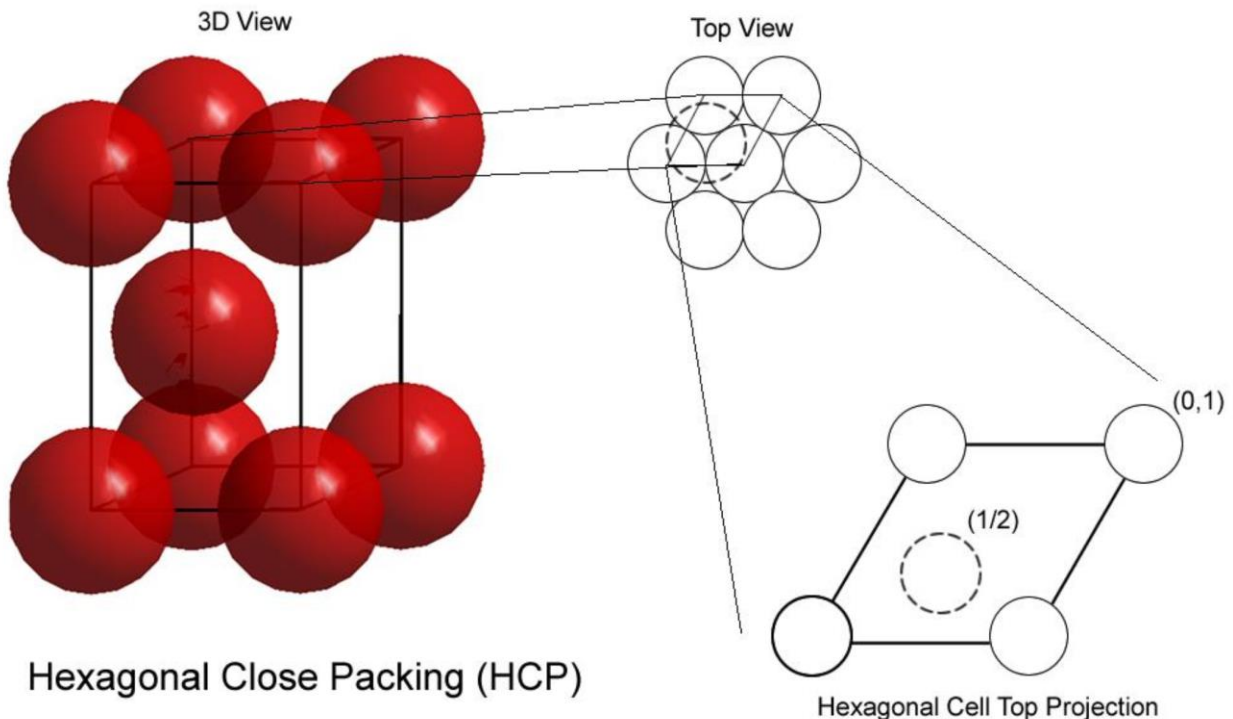
Figure 5: Unit Cell of α-Zr Crystal Structure ("Hexagonal Closed Packing HCP")
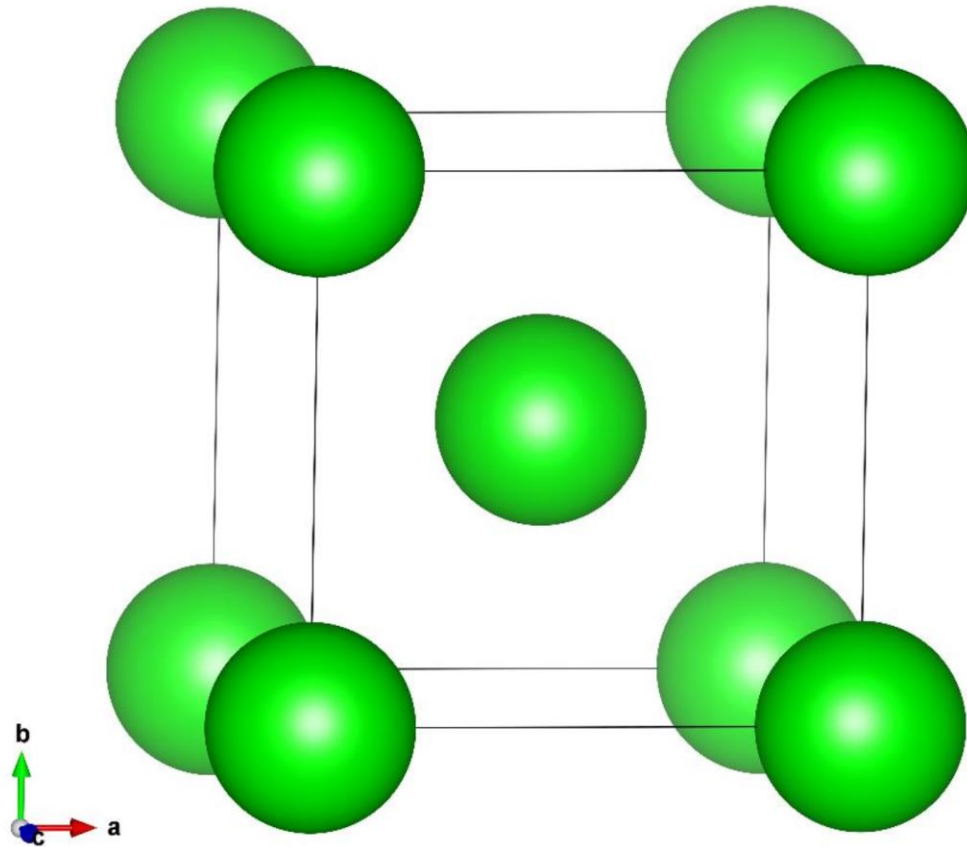
Figure 6: The β-Zr Crystal Structure

Uranium-Zirconium (U-Zr)

Zirconium has long been used in nuclear reactors as cladding and for other components due to multiple properties; it has a high temperature BCC phase, high melting point, very small neutron absorption cross-section, low cost, and high fission product yield. The reasons that make it a good material for reactor components are the same reasons it should make a good material to be alloyed with uranium for metallic alloy fuel. In the past, which metal to alloy with uranium has been decided by trial and error, compromising between corrosion resistance and mechanical properties. In addition to several other candidates, such as molybdenum and niobium, uranium-zirconium has been selected as a great option for nuclear fuel in fast reactors.

At reactor operating temperatures, both uranium and zirconium are in the body centered cubic phase, so all uranium-zirconium alloys, no matter the composition, will be in body centered cubic as well. It should be noted that from 65% to 75% zirconium, the alloy goes through a δ (C32 crystal structure) before transitioning to the predicted γ phase at 890 K. However, this research focuses on alloys up to 30% zirconium. H. Okamoto has created the most recent uranium-zirconium diagram utilizing a compilation of experimental papers, as shown below.
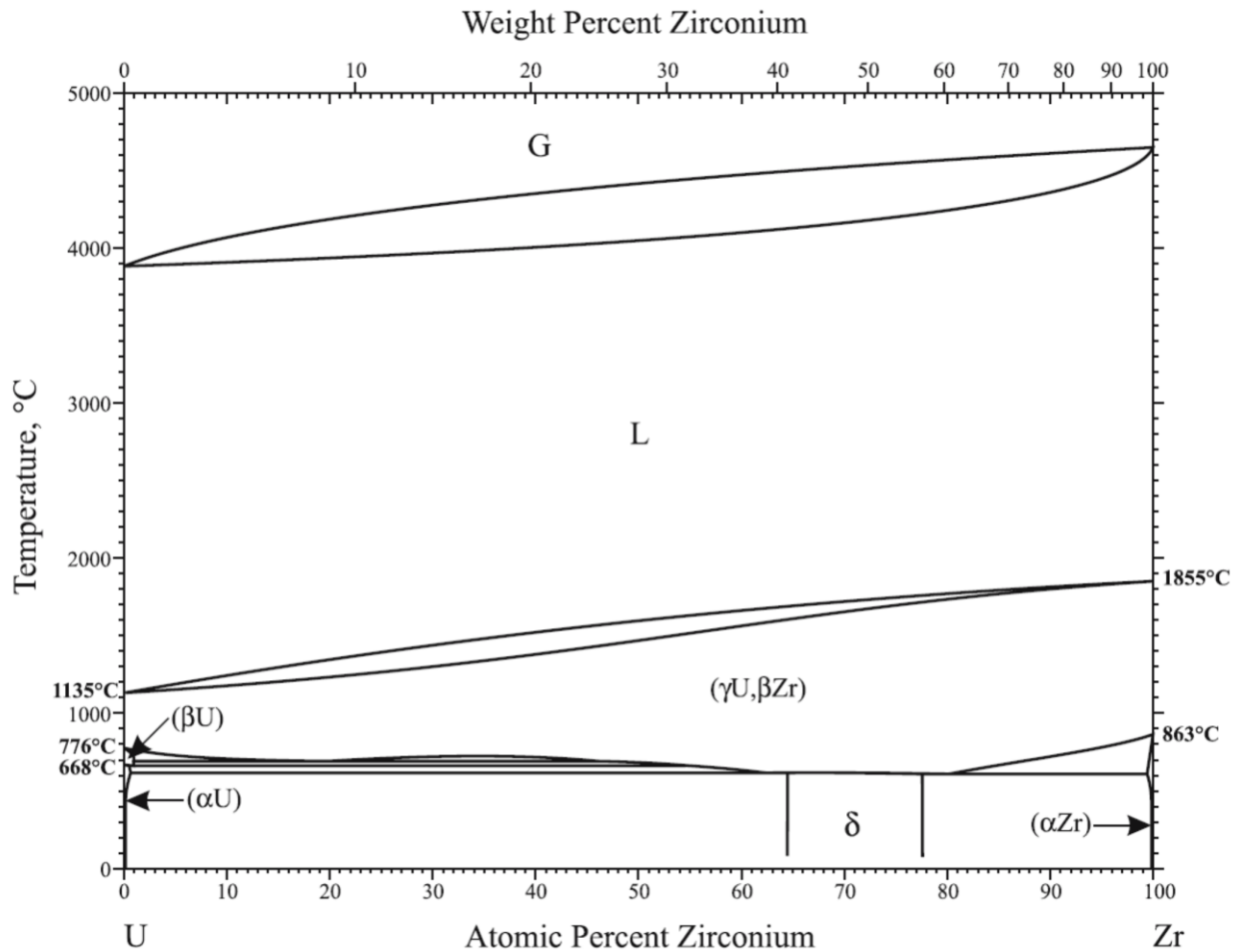
Figure 7: Phase Diagram of U-Zr (Okamoto 2007)

Due to sharing a BCC structure, γU and βZr are completely miscible and the alloy of the two have isotropic neutronics, which is why it is the main phase of interest for high temperature fast reactors. The BCC phase also has the desired isotropic expansion for use in the TRIGA type pool reactors and the Generation IV SFR's reactors (EBR-II, SABR, S-PRISM, etc.), but there is not as much experimental data about the lower temperature phases. The primary focus of this research is the BCC metallic phase.

Applications of Uranium-Zirconium

One of the advanced reactor designs that will be made possible through use of metallic alloy fuels is the Subcritical Advanced Burner Reactor (SABR). In this design, a subcritical fission reactor is driven by a fusion neutron source, similar to a tokamak design. This design has several advantages, such as using not highly enriched fuel and better safety since the design is inherently subcritical (Stacey, unpublished data).
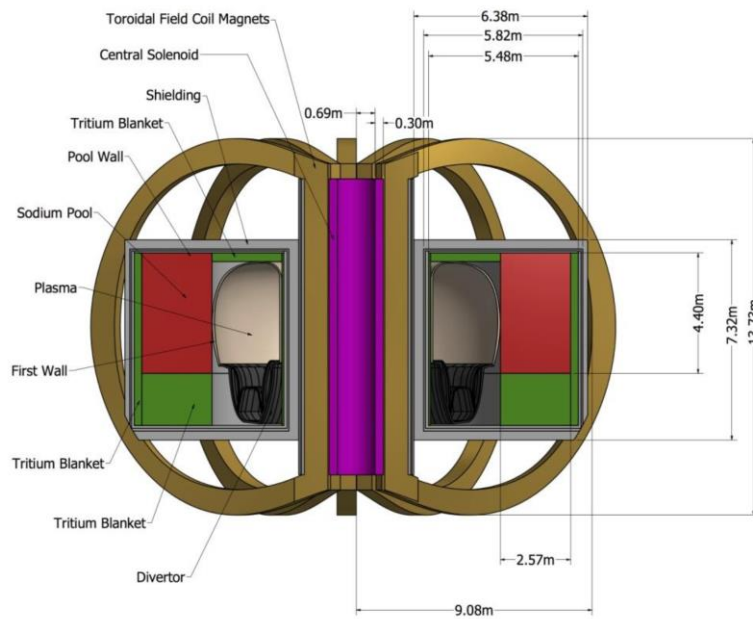
Figure 8: Perspective View of SABR Configuration (Stacey, unpublished data)
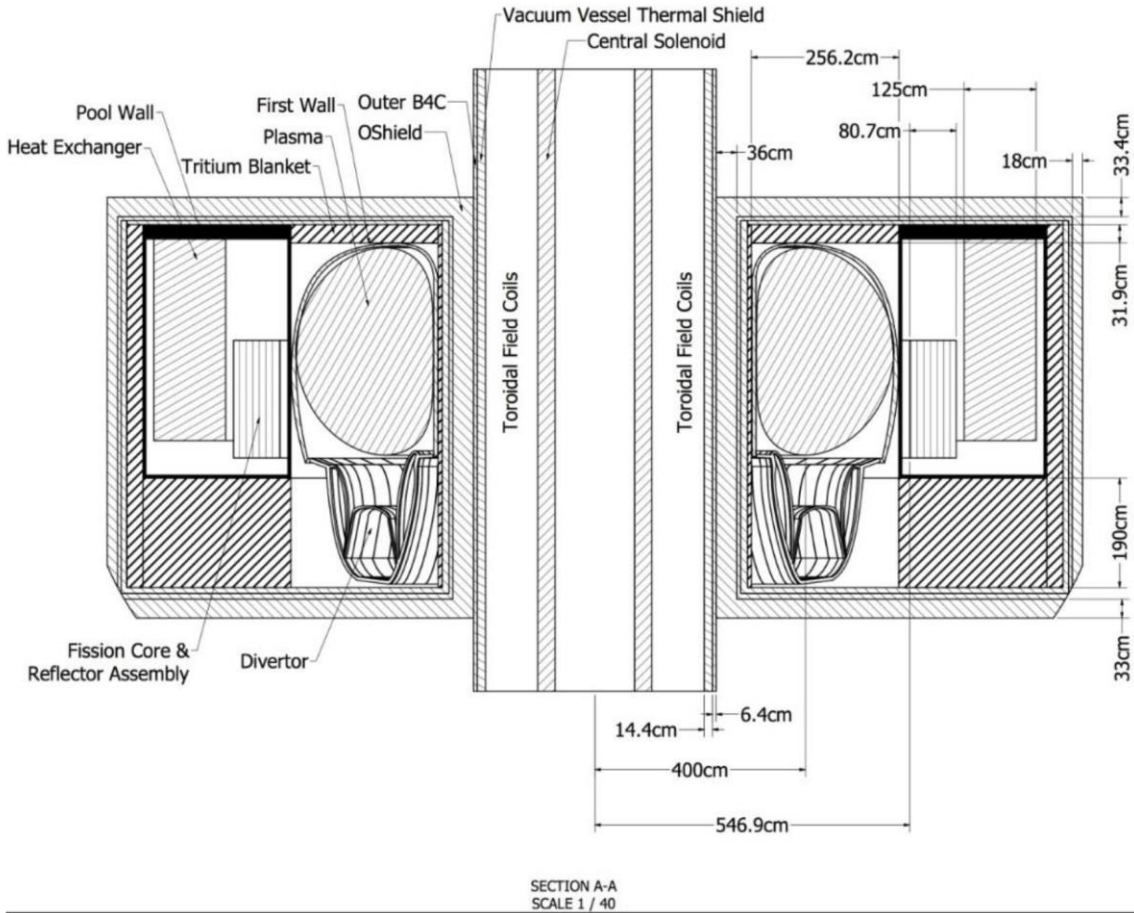
Figure 9: Radial View of SABR Configuration (Stacey, unpublished data)

Table 2: Basic SABR Core Properties (Stacey, unpublished data)

Fast Reactor Core Properties	
Coolant	Sodium (Na)
TRU fuel composition	40Zr-10Am-10Np-40Pu
Fuel Maximum / Allowable Temperature	1014 K / 1200 K
Cladding Maximum / Allowable Temperature	814 K / 923 K
Coolant Maximum / Allowable Temperature	787 K / 1156 K
BOL TRU mass	15104 kg
BOL keff	0.973
Specific power	198.6 W/gHM
Fuel assembly	800
Fuel pin	469/per assembly, 375,200 total

Table 2 Continued: Basic SABR Core Properties (Stacey, unpublished data)

Power density	256 kW/L
Linear fuel pin power	12.3 kW/m
Sodium coolant mass flow rate	16,690 kg/s
Coolant temperature Tincool/Toutcool	628 K/769 K
Fuel & Clad temperature Tmaxfuel/Tmaxclad	1014 K/ 814 K
Clad & Structure	ODS MA957
Electric insulator	SiC
Fuel/Clad/Bond/Insulator/duct/coolant/wire (v/o)	22.3/17.6/7.4/6.5/9.3/35.3/1.5%

However, this design did come with a few problems. SABR is designed for long fuel irradiation cycles with high burn-up, so the metallic alloy fuel would undergo a large amount of swelling and a significant fission gas production. In order to combat this, the fuel is fabricated with a 75% smear density and an extra-long plenum was created to hold the fission gases that escape the fuel. Swelling and fission gas is already an issue with metallic fuels, but with SABR's higher burn-up conditions, the plenum is twice as long as the fuel region, allowing the extra fission gas to escape.
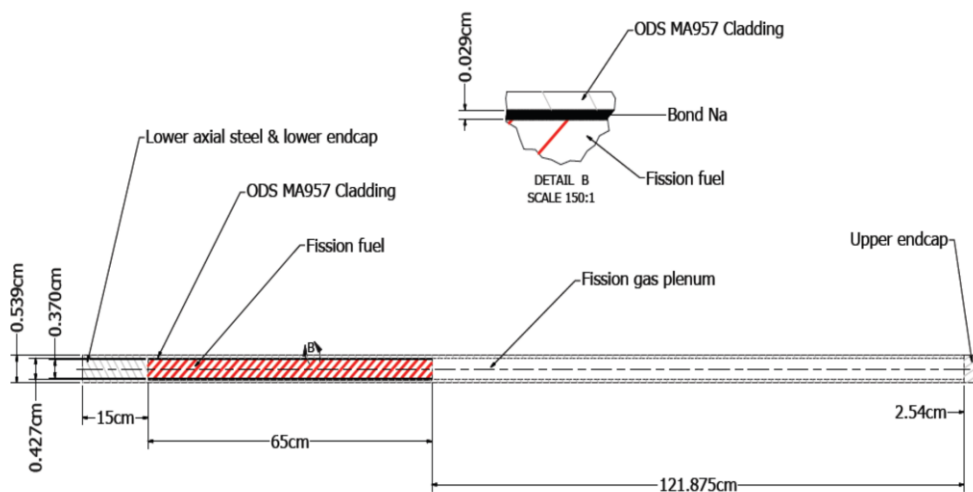
Figure 10: SABR Fuel Pin Configuration (Stacey, unpublished data)

As previously discussed in the Metallic Fuel Disadvantages section, the cladding is also going to be subject to irradiation damage and fuel cladding interactions (FMMI and FCMI). So far, the SABR design keeps the cladding irradiation damage below the set limit; however, incorporating fuel cladding interactions may require more research to keep it below safety limits.

In This Work

The aim of this thesis is to provide vacancy formation energy for various uranium-zirconium alloys in the BCC phase at low temperatures and at operational temperatures, which has not previously been researched due to interest in metallic alloys as fuel being a recent development. In order to do this, a 10x10x10 structure of the alloy was simulated, composed of 2000 atoms total, in the Large-scale Atomic/Molecular Massively Parallel Simulator (LAMMPS) using a Modified Embedded-Atom Method (MEAM) interatomic potential and a vacancy was created in the middle of the structure. The energy of the structure before and after the vacancy was created was used in order to determine the vacancy formation energy.

In addition to calculating vacancy formation energy, several different analysis methods were used to determine how the vacancy, temperature, and alloying affected the overall cohesion of the atomic structure. Short-range order, Wigner-Seitz defect analysis, common neighbor analysis, and the radial distribution function were all used to give insight into how the different factors affect the atomic structure.

Chapter 2: Methods

Computational Simulations

By modeling materials using computer simulations, it is possible to get a much closer look at the properties of the materials than just through experimentation. Using computational methods, one can see the effect removing or adding one single atom to the lattice structure has, or at what precise moment a material changes phase. Without thorough information on the microstructural properties only obtainable through computational methods, it is much more difficult to predict how the macroscopic properties will react under varying circumstances.

Ensembles are composed of a group of atoms, represented by a sequence of points, that satisfy the conditions of a particular thermodynamic state. An ensemble can have atoms with many different microscopic states, but are unified by one or more macroscopic or thermodynamic property.

Ensembles are named after the properties that are fixed, or the independent variable. Not only would not holding any of the variables constant be computationally expensive, but it would be difficult to interpret the data and which changing property is affecting the thermodynamic properties of the whole structure. Ensembles are in computational simulations in order to find the approximate equilibrium state of the dependent variables.

In order to calculate the equilibrium values of the dependent variables, it is assumed that once the simulation has undergone enough steps, the dependent variables will be fluctuating

around the equilibrium value, so the average of the value is taken once the dependent value has started fluctuating until the end of the simulation. The equation is shown below

$$\langle A \rangle = \sum_i A_i p_i \qquad (1)$$

It is assumed that the ensemble average is the same as the time average once the variations of the dependent variables have settled to fluctuate around the equilibrium value; this is known as the Ergodic hypothesis for Molecular Dynamics simulations.

$$\langle A \rangle = \lim_{t \to \infty} \frac{1}{t} \int_0^t A \, dt \qquad (2)$$

Table 3: Common Thermodynamic Ensembles

Ensembles	Independent Variables	Dependent Variables	Z (Partition Function)	Pi (ith state Probability)
Microcanonical	N, V, U	μ, P, T	$\sum_i \delta(E_i - E)$	$\dfrac{\delta(E_i - E)}{Z_{NVE}}$
Canonical	N, V, T	μ, P, E	$\sum_i e^{-\beta E_i(N,V)}$	$\dfrac{e^{-\beta E_i(N,V)}}{Z_{NVT}}$
Grand Canonical	V, T, μ	N, P, L	$\sum_i e^{\beta N \mu} Z_{NVT}$	$\dfrac{e^{-\beta(E_i - \mu N)}}{Z_{NV\mu}}$
Isothermal-Isobaric	N, P, T	μ, V, H	$\sum_i e^{\beta p V_i} Z_{NVT}$	$\dfrac{e^{-\beta(E - pV_i)}}{Z_{NPT}}$

The total energy of the system is U, $\beta = 1/k_B T$ is the reduced temperature, Z is the partition function, N is the number of moles, V is volume, T is temperature, μ is the chemical potential, P is the pressure, H=U+PV is the enthalpy, L=U - $\Sigma(\mu_i N_i)$ is the Hill energy, P_i represents the probability of observing the ith state, and all of the other subscript i's represent the parameter at the ith state (Hünenberger 2005).

Molecular Dynamics

Molecular Dynamics computational methods utilizes an interatomic potential in order to properly simulate how the atoms in a structure interact with each other. In this case specifically, the Modified Embedded-Atom Method (MEAM) was used, but more on that later. Molecular Dynamics uses the gradient vector of the potential energy at each atom's location to determine the force acting upon that atom. This force is specifically calculated using the MEAM interatomic potential. In Molecular Dynamics, each atom is allowed to move for a short period of time based on the forces being applied to it by the other atoms, as calculated by the MEAM interatomic potential. Molecular Dynamics then gives snapshots of the structure over time as the atoms are allowed to move around until they have come to an equilibrium state. The temperature of the simulation is calculated based on the average velocity of all of the atoms.

The Large-scale Atomic/Molecular Massively Parallel Simulator (LAMMPS) was the Molecular Dynamics code used in this research. The initial setup consisted of 2000 atoms with periodic boundary conditions in an unrelaxed, perfect BCC lattice. The atoms were then allowed to relax by running in an isothermal-isobaric (NPT) ensemble, where the number of atoms, pressure, and temperature are held constant. Then, the center atom is removed and the remaining 1999 atoms are run in a canonical (NVT) ensemble, where the number of atoms, volume, and temperature remained constant.

Modified Embedded-Atom Method Interatomic Potential

Interatomic potentials are of vital importance to simulations that model material properties. The foundation of these potentials is Density Functional Theory (DFT), which posits that energy is a functional of the electron density. With knowledge of the electron density of an entire system, one can determine the potential energy of a system:

$$U = f[\rho(r)] \tag{3}$$

$$E[\rho(r)] = T_s[\rho(r)] + J[\rho(r)] + E_{xc}[\rho(r)] + E_{ext}[\rho(r)] + E_{ii}[\rho(r)] \tag{4}$$

where E is the total energy, T_s is the single particle kinetic energy, J is the Hartree Electron-Electron Energy, E_{xc} is the Exchange Correlation Functional, E_{ext} is the Electron-Ion Coulombic Interaction, and E_{ii} is the Ion-Ion Energy (Moore 2013).

With this basis, the Embedded-Atom Method (EAM) was created by assuming that an atom can be embedded into a homogeneous electron gas, and the change in potential energy is a functional of the embedded atom electron density that can be approximated with an embedding function. In a crystal, though, the electron density is not homogeneous, so the EAM potential replaces the background electron density with the electron densities for each atom and supplements the embedding energy with a repulsive pair potential to represent atoms core-core interactions.

With a simple linear superposition of the atoms' electron densities as the background electron density, the EAM is governed by the following equations:

$$R_{ij} = |r_i - r_j| \tag{5}$$

$$\bar{\rho}_i = \sum_j \rho_j^a(R_{ij}) \tag{6}$$

$$U = \sum_i F(\bar{\rho}_i) + \frac{1}{2}\sum_{i,j} \phi(R_{ij}) \tag{7}$$

where R_{ij} is the distance between atoms i and j, ρ_j^a is the atomic electron density, r_i is the position of atom i, F is the embedding function, ρ_i are the electron densities, and ϕ is the pair interaction potential.

However, EAM does not do a great job of simulating materials with significant directional bonding, which includes most metals. In order to properly simulate metals, the Modified Embedded-Atom Method was created, which allows the background electron density

to depend on the local environment instead of assuming a linear superposition. The equation governing the potential energy is

$$U = \sum_i F(\bar{\rho}_i) + \frac{1}{2}\sum_{i,j \neq i} \phi_{ij}(R_{ij})S(R_{ij}) \qquad (8)$$

The main difference between the equation for potential energy for the EAM and MEAM is the inclusion of S, which is the radial screening.

For a MEAM interatomic potential that describes the relationship for alloys with two or more components, each individual component needs 13 individual adjustable parameters. In addition, every binary interaction needs at least 14 adjustable parameters. These parameters are used in the calculation of the potential energy described in equation 8 and govern the forces that are acting upon the atoms. (Moore, 2016) These parameters are given below in Tables 4 and 5.

Table 4: Single Element Parameters

Parameter	Uranium	Zirconium
A	0.98	0.48
β^0	4.8	2.8
β^1	6	2
β^2	6	7
β^3	6	1
t^1	2.5	3
t^2	4	2
t^3	1	-7
α	5.1	4.1
δ	0.105	-0.03
Ec	5.27	6.2
C_{min}	1	0.7
C_{max}	1.9	0.99

Table 5: Binary Interactions

Parameter	Uranium-Zirconium
δ	0.05
α	4.8
r_e	2.85
ρ_U	1.2
ρ_{Zr}	0.8
Δ	0.8
$C_{min}(U,Zr,U)$	0.8
$C_{min}(Zr,U,U)$	0.5
$C_{min}(Zr,Zr,U)$	0.5
$C_{min}(Zr,U,Zr)$	0.5
$C_{max}(U,Zr,U)$	2.5
$C_{max}(Zr,U,U)$	2
$C_{max}(Zr,Zr,U)$	2.8
$C_{max}(Zr,U,Zr)$	2.8

MD Time Converging and Averaging

As previously discussed, the simulation must first be run long enough for dependent variables of the ensemble to settle from the initialized position. Once that has happened, they also must be run long enough to give a statistically sound average. For both before and after the center atom of the lattice structure is removed, the simulation is run for 20 picoseconds with a timestep of 1 femtosecond, which gives 20,000 steps for each stage, and 40,000 steps total. The ensemble average of the properties was calculated during the last 10 picoseconds of each stage.

Periodic Boundary Conditions and Finite Size Effects

In order to allow a small lattice structure of 2000 atoms to properly represent a full sized structure, a periodic boundary condition is used so that if an atom leaves one end of the cell, it returns on the opposite side, as if a new atom came in to take its place. This ensures that the lattice always has the proper number of atoms while also simulating a much larger structure.

Even with the periodic boundary conditions, the system must be large enough to accurately represent the effects of all of the atoms that are close enough to apply a force to the atom that is removed for the vacancy. However, the larger the computational system, the even longer the computational time becomes, leading to need to find a "sweet spot" between reducing both periodic boundary finite size effects and computational runtime.

Finite periodic box size effects can be hard to quantify, especially due to thermal scattering events dominating the finite periodic box effects. A larger box size also leads to better time averages thanks to the law of large numbers. The box size also needs to be large enough to allow separation, clustering, and ordering effects to be seen without neighboring reflected images interfering.

A 10x10x10 BCC unit cells cubic periodic box was chosen based upon previous research which analyzed the potential energy from a random solid solution molecular dynamics simulation over a range of sizes to find a proper size to keep the periodic boundary finite size effects to a minimum (Moore 2013). The 10x10x10 unit cells form a supercell. It is recommended that the size of the structure is larger than twice the cutoff distance to reduce PBC, and 10x10x10 is much larger. This condition is set because it makes it impossible for a particle to be under the effect of two images of a different, given particle.

Alloying

Several different atomic percentage alloys are used throughout here; 0%, 10%, 20%, and 30% zirconium alloys. In real life, alloys are never exactly the correct atomic percentage. In order to properly simulate this, atoms were changed at random. Starting with a pure uranium 10x10x10 BCC structure, each atom was given a chance at becoming zirconium, that chance being the desired atomic percentage of zirconium in the structure. In addition, to ensure that one

random seed number doesn't affect the results too far away from the desired atomic percentage, five different structures were created for each desired atomic percentage, allowing for actual atomic percentages above and below the desired one.

Vacancy Formation Energy

In order to calculate a vacancy formation energy, a single vacancy was introduced into a perfect lattice with equilibrium lattice constants and structural relaxation of atomic positions. Only non-interacting isolated defects were considered when calculating defect formation energy. Visual verification and common neighbor analysis was also used to ensure that the structure of the lattice did not alter phase once the defect had been introduced. With periodic boundary conditions and no point-defect sources, the only other types of defects that could form during the simulation were vacancy-interstitial pairs (Mendelev 2009).

Generally, the formation energy of a vacancy in a homogeneous bulk crystal that does not change phase can be described by:

$$E_v = E_{(n-1)} - \left[\frac{n-1}{n}\right] E_n \tag{9}$$

$E_{(n-1)}$ is the total energy of an atom supercell containing one vacancy, while E_n is the total energy of that supercell before the vacancy was created.

In this research, the vacancy formation energy was calculated by taking averages in three different ways. In the first way, the total energy from the last 10,000 MD steps of each stage was averaged before plugging into equation 3. Similarly, the variance was calculated for each of the two stages before being used to calculate the overall variance from equation 3 as shown in equation 10:

$$\sigma = \sqrt{\sigma_{(n-1)}^2 + \left[\frac{n-1}{n}\right]^2 \sigma_n^2} \tag{10}$$

The second method was to calculate the total energy per atom in each of the 10,000 MD steps, as shown in equation 11:

$$E_{atom} = \frac{E}{n} \qquad (11)$$

where n is either 2000 or 1999, depending on whether or not the vacancy had been introduced. The energy per atom of each step is then averaged and those values were used in equation 9. For the error, the variance of the energy per atom of each step was calculated, and then those values were used in equation 10. The final method had the difference in total energy calculated for each individual step, as shown in equation 12:

$$E_{v,i} = E_{(n-1),i} - \left[\frac{n-1}{n}\right] E_{n,i} \qquad (12)$$

Then, the total vacancy formation energy is calculated:

$$E_v = \frac{\sum_{i=1}^{10,000} E_{v,i}}{10,000} \qquad (13)$$

The error is calculated simply by taking the variance of the results from equation 12.

Short Range Order Parameter

Order parameters allow the configuration and order of a structure to be quantified in simple, easy to comprehend values without even looking at the structure itself. The Short Range Order (SRO) parameter uses only the atoms' first nearest neighbors in order to give a single digit to represent the order of the structure:

$$\sigma = -\frac{P_{AA} - n_A}{1 - n_A} \qquad (14)$$

Here, P_{AA} is the fraction of nearest neighbor sites of atom type A that are occupied by A type atoms (averaged over all A type atoms) and n_A is the total atom fraction of A type atoms in the whole system.

So, for the SRO parameter, for a system with an equal number of A and B atom types, a perfectly ordered lattice has a σ = 1, a phase separated system has a σ = -1, and a totally random solid solution has a σ = 0. If the A and B atom types are unequal, σ's extreme values, perfect order and phase separated, are reduced in magnitude.
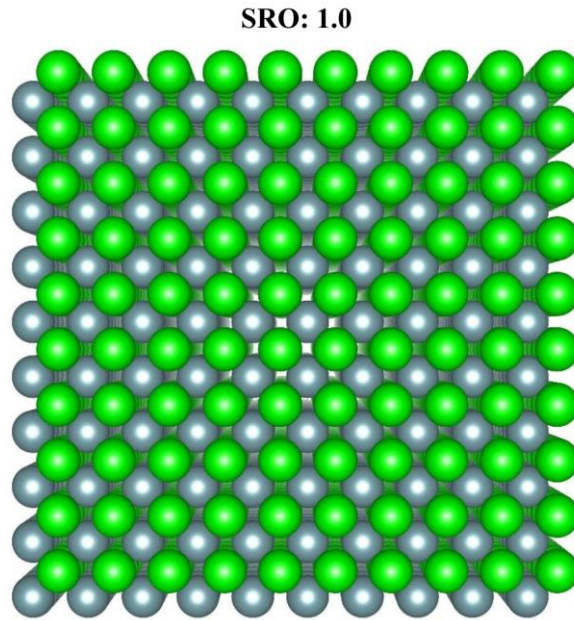
Figure 11: Perfectly Ordered Periodic B2 U-Zr System (Uranium 50% atomic fraction and Zirconium 50% atomic fraction) (Moore 2013)

SRO: -0.8
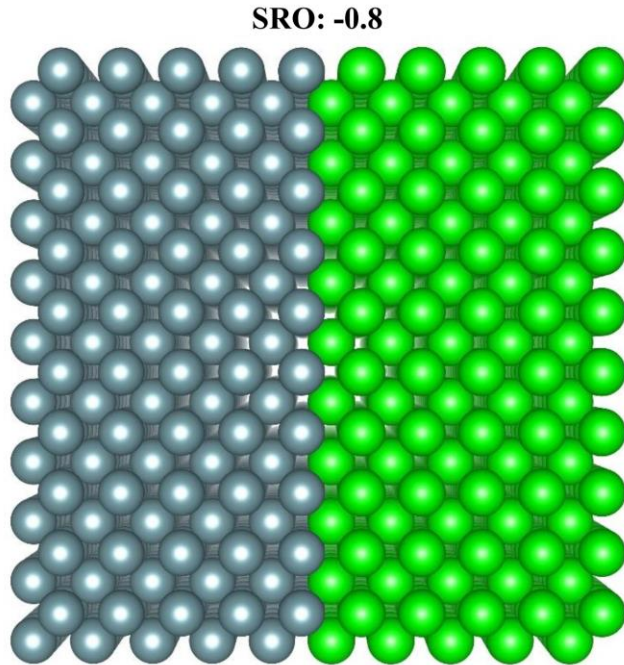
Figure 12: An Example of a Periodically Separated U-Zr System (Uranium 50% atomic fraction and Zirconium 50% atomic fraction) (Moore 2013)

Because this work uses a finite box with periodic boundary conditions, it is impossible to have an SRO of $\sigma = -1$. In this case, the separated SRO parameter depends on the box size and the way the atoms separate; it is possible for the atoms to separate and be divided by a single planar line (see above) or to be clustered into a bunch.

Figure 13: An Example of a Configuration of a Plane of Atoms Not Captured by the Short Range Order Parameter

Because the Short Range Order parameter is a simple quantified representation of a potentially complex order, it is possible that some configurations are not properly represented by the single number. For this reason, visual verification should always be performed i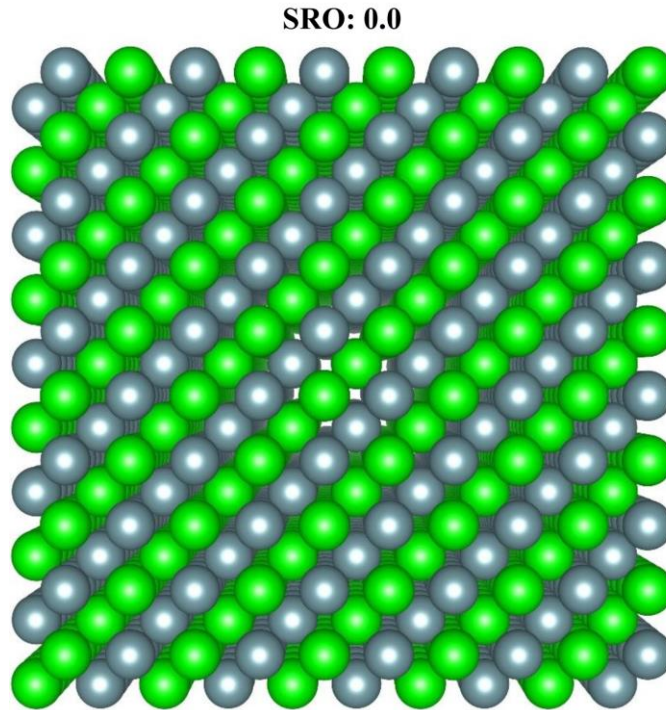n addition to calculating the Short Range Order parameter. For instance, alternating planes of atoms will not be obvious just from the parameter.

The Short Range Order parameter code assumes a Body Centered Cubic crystal structure, which means each atom has eight nearest neighbors. The order parameter is calculated on a snapshot of the atoms' position at any time.

Wigner-Seitz Defect Analysis

Wigner-Seitz defect analysis was used to determine whether or not point defects formed during the simulation run. This defect analysis works by taking a reference state, in this case, the initial, perfect 10x10x10 BCC structure before relaxation occurs, and comparing it to the

displaced configuration, the rest of the timesteps occurring during the simulation, both before and after the vacancy was created.

Wherever a particle is located in the refence state is defined as a Wigner-Seitz cell, which is the spatial region belonging to that site. The defect analysis compares the displaced configuration to the reference state; if there are no particles within a Wigner-Seitz cell, that cell contains a vacancy, if there is one particle, then the cell is normal, and if there are more than one particles within the cell, the cell contains an excess interstitial.

Due to the periodic boundary conditions and no point-defect sources, the structure before the vacancy is created will always have the same number of vacancies and interstitials, known as vacancy-interstitial pairs, while once the vacancy has been created, there will always be one more vacancy than interstitials.

Common Neighbor Analysis

In order to determine whether or not the alloys maintain their phase during the simulations, Common Neighbor Analysis was used to verify this. Common Neighbor Analysis, developed by Honeycutt and Andersen, uses an algorithm to develop a "fingerprint" for pairs of atoms, which characterizes the local structural environment. CNA allows an accurate understanding of which particles are part of which phase, and which are near defects.

Original Common Neighbor Analysis used a cutoff distance to determine whether or not a pair of atoms were bonded, but Stukowski was able to develop an adaptive CNA, which automatically determines cutoff distances for each particle. This allows the parts of the structure which may have slightly changed phase to be determined more readily.

Radial Distribution Function

The radial distribution function gives the density of surrounding particles around each particle and averages them, giving a function that describes, on average, how close particles are to each particle. It is calculated by showing how the atomic density from a reference particle varies as a function of radial distance from the reference particle.

$$g(r) = \frac{1}{4\pi N r^2 \rho_0} \sum_{j=1}^{N} \sum_{\substack{i=1 \\ i \neq j}}^{N} \delta(r - r_{ij}) \tag{15}$$

This equation gives the probability of finding a particle in the distance r from a given particle.

A lot of useful information can be pulled from equation 9. By looking at the width of the peaks, one can determine the average thermal scatter, and by examining the distance between the peaks, one can find the phase of the system. It is even possible to determine the chemical ordering of a complex system if elemental radial distance functions are used.

Vacancy Formation Energy

As discussed in the methods section, the vacancy formation energy was calculated using three different methods; the first and third methods used the total energy of the atomic structure, while the second method used the per-atom energy by dividing the total energy by the number of atoms currently in the lattice. As a result, the first and third methods provide incredibly similar results, which are also on the same order of magnitude as previous literature on uranium's vacancy formation energy. Consequently, the first method will be the one used for all subsequent plots. Table 6 gives the results of using all three methods for calculating the vacancy formation energies and standard deviations for all simulation cells run at 800 K. This includes all five cells run at each of zirconium atomic percentages. This demonstrates the similarities of method 1 and 3 and the vastly different method 2.

Table 6: Vacancy Formation Energies for 800 K

	800	Zr00	Zr10	Zr20	Zr30
1	Average 1	1.4003428	1.72230583	2.312345965	-4.178796141
	STD1	2.257896704	2.688173452	2.902574502	3.607615093
	Average 2	-0.001908113	-0.001760533	-0.001495244	-0.004785475
	STD2	0.00112919	0.001344426	0.0014516	0.001804203
	Average3	1.4003428	1.722305831	2.312345965	-4.178796141
	STD3	2.170656194	2.595606021	2.804284086	3.574143694
2	Average 1	1.720643487	2.053608134	1.722105598	-1.133259236
	STD1	2.022735887	2.531301846	2.927282985	3.248059382
	Average 2	-0.001747883	-0.001590306	-0.001787191	-0.003242758
	STD2	0.001011637	0.001266019	0.001464008	0.001624444
	Average3	1.720643487	2.053608134	1.722105598	-1.133259236
	STD3	2.115359269	2.525967153	2.709120597	3.257120844
3	Average 1	1.689327583	2.304935836	-0.547867803	-6.774253473
	STD1	2.101852991	2.675434503	2.781539863	3.324777606
	Average 2	-0.001763556	-0.001469821	-0.002921053	-0.00607661
	STD2	0.001051216	0.001338043	0.001391046	0.001662844
	Average3	1.689327583	2.304935836	-0.547867803	-6.774253473
	STD3	2.161064914	2.682473845	2.618852329	3.025901579
4	Average 1	1.359732973	1.71248722	2.548949382	1.724600213
	STD1	2.060468302	2.760003622	3.113229914	3.072065616
	Average 2	-0.00192837	-0.001763649	-0.001379558	-0.001827037
	STD2	0.001030463	0.001380338	0.001557022	0.001536396
	Average3	1.359732973	1.71248722	2.548949382	1.724600214
	STD3	2.109341858	2.700361996	2.931444244	3.112080664
5	Average 1	1.691577218	2.771411018	2.094677183	-0.937796166
	STD1	2.356761998	2.746576606	2.963672623	3.342092555
	Average 2	-0.001762432	-0.001233841	-0.001600171	-0.00315786
	STD2	0.001178665	0.001373582	0.001482204	0.001671461
	Average3	1.691577218	2.771411018	2.094677183	-0.937796166
	STD3	2.402609671	2.706361126	2.967630712	3.099820388

For method 1, the total energy of the perfect lattice was calculated by averaging the total energy of the last 10,000 timesteps before the vacancy was introduced. The total energy of the lattice with a vacancy was also calculated by averaging the total energy of the last 10,000 timesteps after the vacancy was introduced. The vacancy formation energy was the calculated using equation 9, repeated below:

$$E_v = E_{(n-1)} - \left[\frac{n-1}{n}\right] E_n \qquad\qquad (9)$$

where E_n is the total energy of the perfect lattice, $E_{(n-1)}$ is the total energy of the lattice with a

vacancy, and n is the total number of atoms in the structure, 2000. Table 7 gives the average of

the vacancy formation energy for all the temperatures and atomic percent compositions over all

five simulations run for each state.

Table 7: Vacancy Formation Energies Calculated Using Method 1

Temp	Zr00	Zr10	Zr20	Zr30
100	-3.333174385	-0.511642805	-0.414206217	-1.440200866
200	-3.044087069	0.422517349	-0.903291653	-1.53660397
300	-1.63464457	1.083699889	0.212259949	-1.874586013
400	-0.485557605	1.16231472	1.076516211	-0.316028245
500	0.086958022	1.470468981	0.972018486	-3.874073751
600	0.856185428	1.746645698	1.548411563	-0.117170697
700	1.285104182	2.069903275	1.461067739	-4.541624199
800	1.572324812	2.112949608	1.626042065	-2.259900961
900	1.799359394	2.379986064	1.167058059	-11.83625143
1000	2.153252159	2.551729845	1.621974316	-12.95504156
1100	2.513527751	2.592697137	1.787654884	-6.701904151
1200	2.646341879	2.819289136	2.118303777	-4.027482191
1300	2.852343146	3.087606225	0.928831125	-13.07436566
1400	3.034759937	3.058890675	1.592596337	-7.988685364

When looking at the vacancy formation energies the different alloys over temperature, it

is seen that the vacancy formation energies come out negative for the low temperatures. This is

due to the fact that BCC uranium does not actually form until 1045 K. With the phase not

necessarily existing at such low temperatures, it is much more likely for a negative vacancy

formation energy. As the temperature goes up, the vacancy formation energy tends to find a

value similar to those previously reported in the literature, usually between 1 – 2 eV for both

pure uranium and zirconium. However, this is not always the case. With 30%-Zr, the vacancy

formation energies never reach a positive value and the 20%-Zr alloys start to dip a little at

higher temperatures. At high temperatures in BCC phase uranium, there is an increase in the

formation of vacancy-interstitial pairs. The creation of these pairs increases both $E_{(n-1)}$ and E_n,

but increases E_n more. For a relatively small simulation cell where vacancy interstitial pair

formation is rare and the simulation cell will either have one vacancy-interstitial pair or none.

Once a pair has formed, the pair cannot annihilate unless the interstitial and vacancy meet again.

But if the simulation cell already had a vacancy, the vacancy-interstitial pair would exist for a

shorter time because the interstitial now has two vacancies to meet and remove the pair.

Therefore, the energy of the perfect lattice, E_n, is increased more because vacancy-interstitial

pairs last longer there (Mendelev 2010). In fact, if you look at Figures 37 and 38 (in the Wigner-

Seitz defect section) showing the number of defects in the simulation cell at the end of both the

perfect and vacancy stage, you will see that the number of defects go up with temperature and

with the amount of zirconium in the alloy. The effect of formation of vacancy-interstitial pairs on

the vacancy formation energy can be seen in both the figures over change in temperature and in
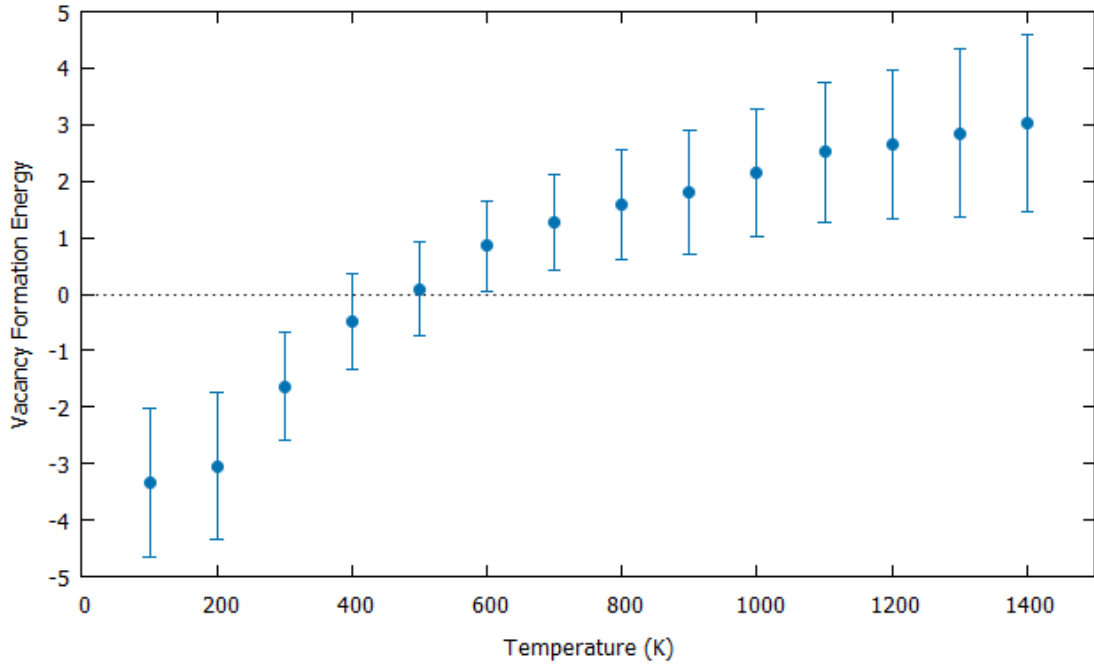
zirconium composition of the alloy.

Figure 14: Vacancy Formation Energy vs Temperature for 0%-Zr

Figure 14 shows the vacancy formation energy for pure uranium. As expected, at very low temperatures where γ-uranium doesn't exist, the vacancy formation energy tends to be negative. Starting a few hundred degrees below the BCC phase transition temperature, there start to be values similar to values previously found in the literature, usually between 1-2 eV.
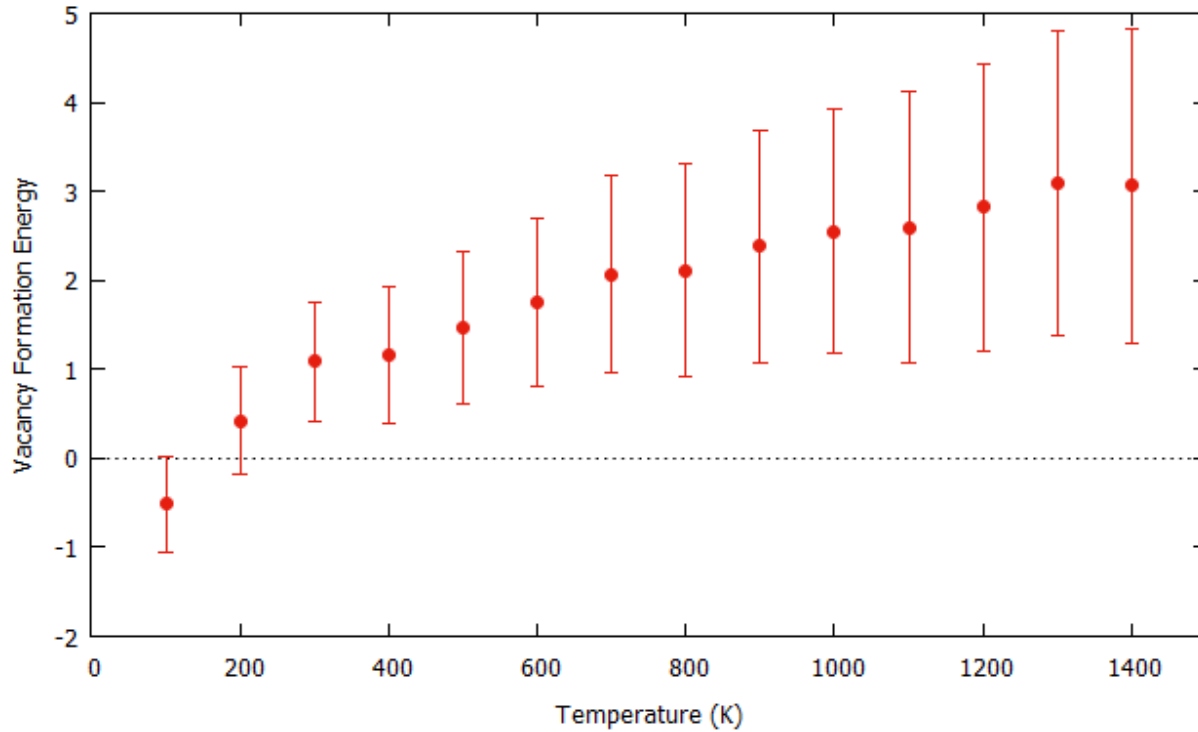
Figure 15: Vacancy Formation Energy vs. Temperature for 10%-Zr

Figure 15 is similar to Figure 14 except that expected values begin to appear at lower temperatures. It is possible that the uranium-zirconium alloy's BCC phase is more stable at lower temperatures. The vacancy formation energies are also still close to vacancy formation energies found for pure uranium and pure zirconium in the literature.
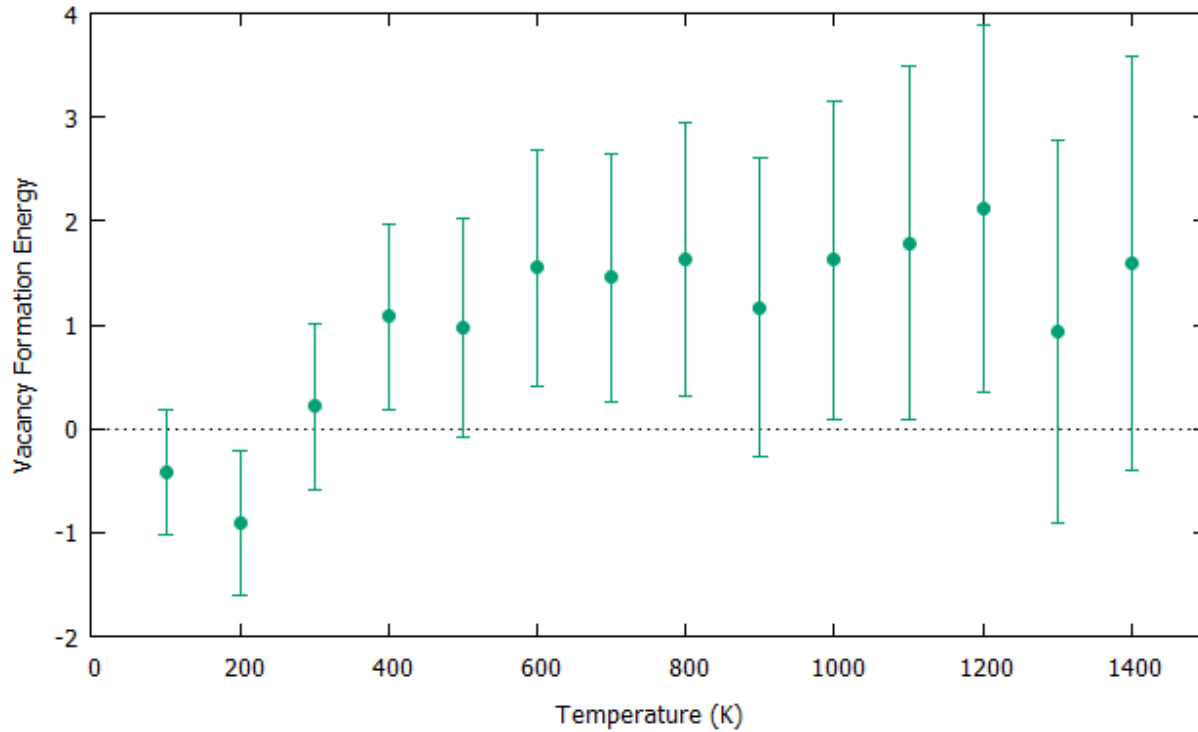
Figure 16: Vacancy Formation Energy vs. Temperature for 20%-Zr

Figure 16 follows a similar trend to Figures 14 and 15, however at higher temperatures the effect of the formation of vacancy-interstitial pairs begin to make itself known as we see oscillating vacancy formation energies as the temperature increases instead of steadily increasing vacancy formation energies. However, again, we still see that at temperatures we would expect the BCC phase to be stable, the vacancy formation energies are around values that have been found previously in the literature for pure uranium and zirconium.
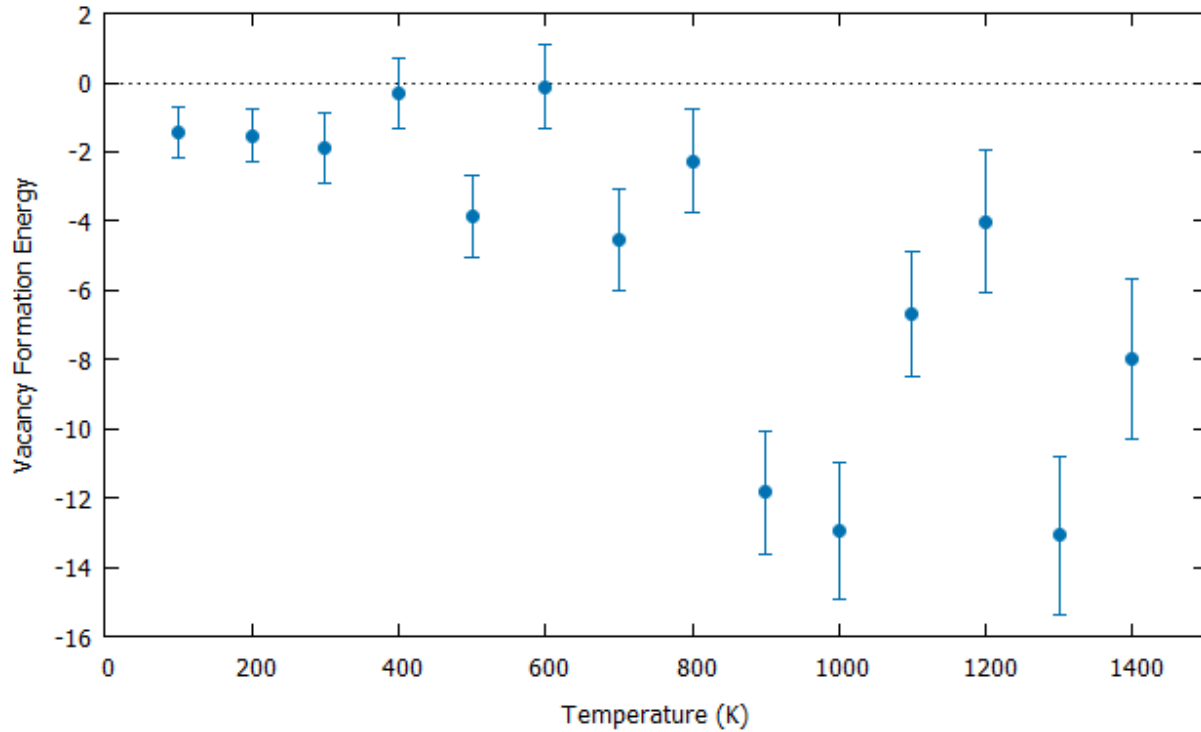
Figure 17: Vacancy Formation Energy vs. Temperature for 30%-Zr

Figure 17 completely bucks the trend established in Figures 14-16 of more or less increasing vacancy formation energies as the temperature of the simulation increases. As will be shown below in the Wigner-Seitz defect analysis, this is almost certainly due to rampant creation of vacancy-interstitial pairs in the 30%-Zr alloy. It seems that the more zirconium included in the alloy, the more easily vacancy-interstitial pairs are created. This effect will be seen throughout the rest of the results presented here.
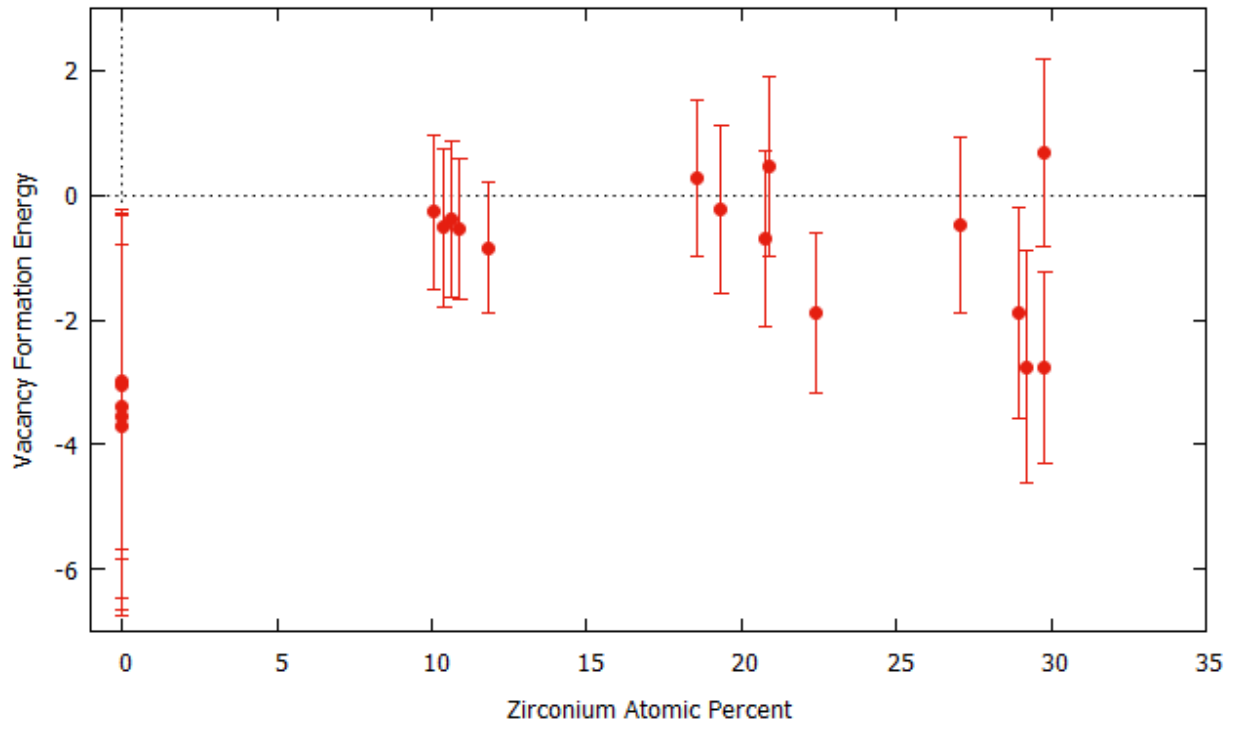
Figure 18: Vacancy Formation Energy vs. Zirconium Atomic Percent for 100 K
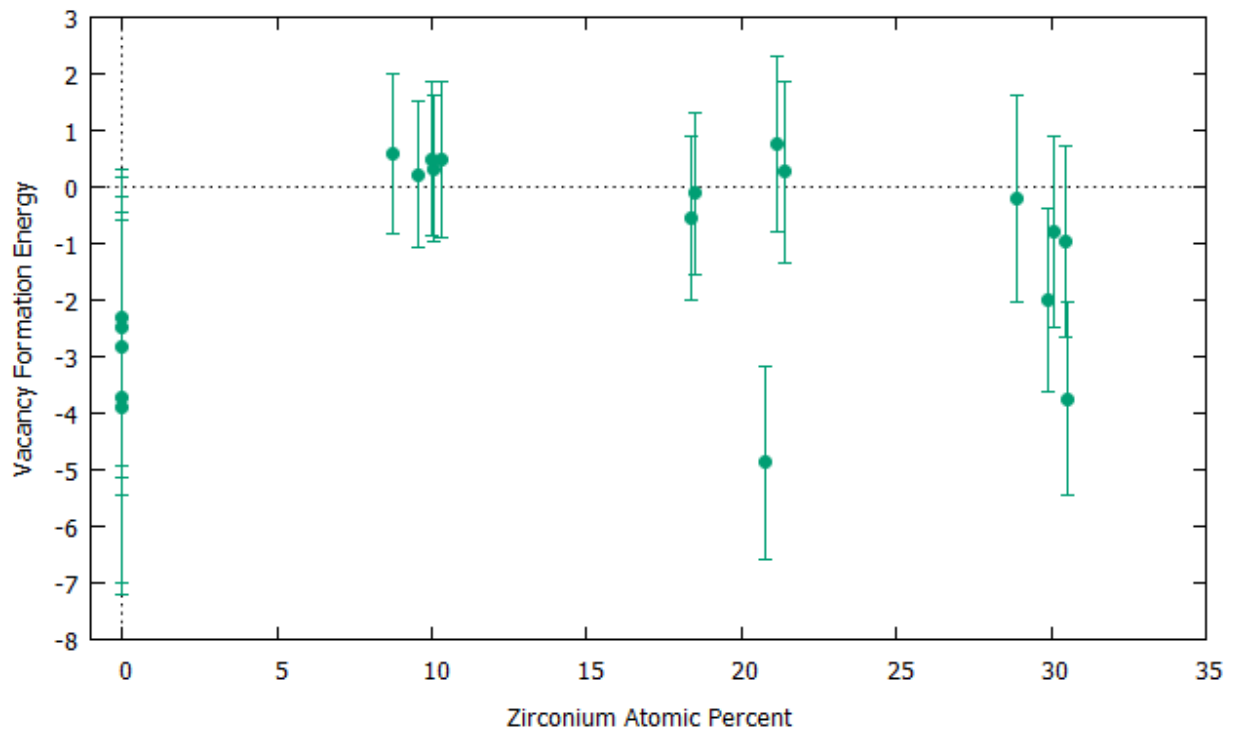

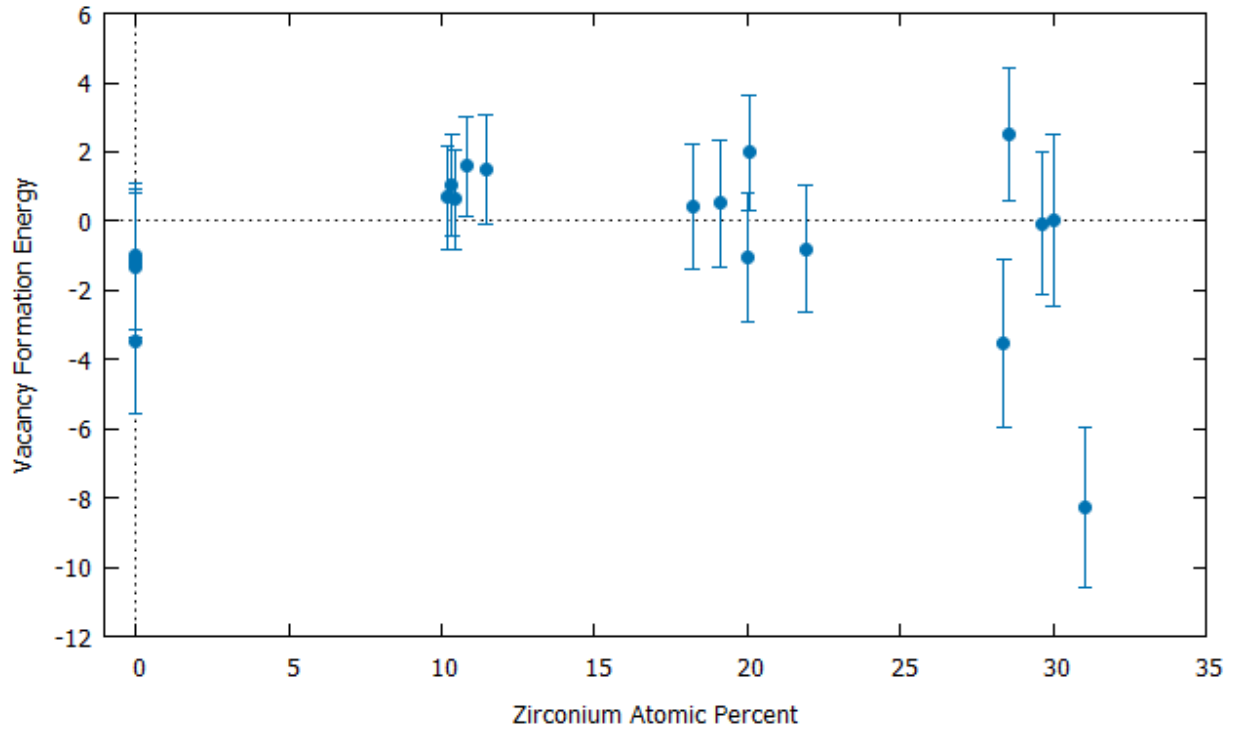Figure 19: Vacancy Formation Energy vs. Zirconium Atomic Percent for 200 K

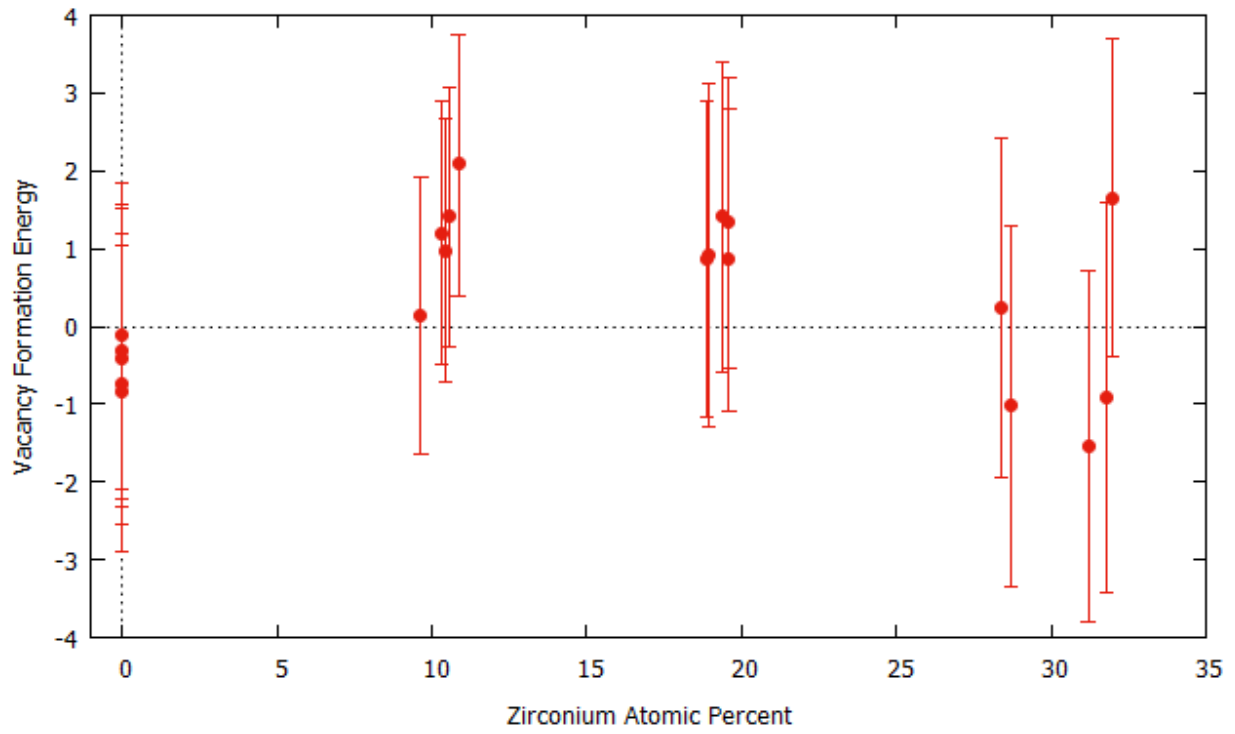Figure 20: Vacancy Formation Energy vs. Zirconium Atomic Percent for 300 K

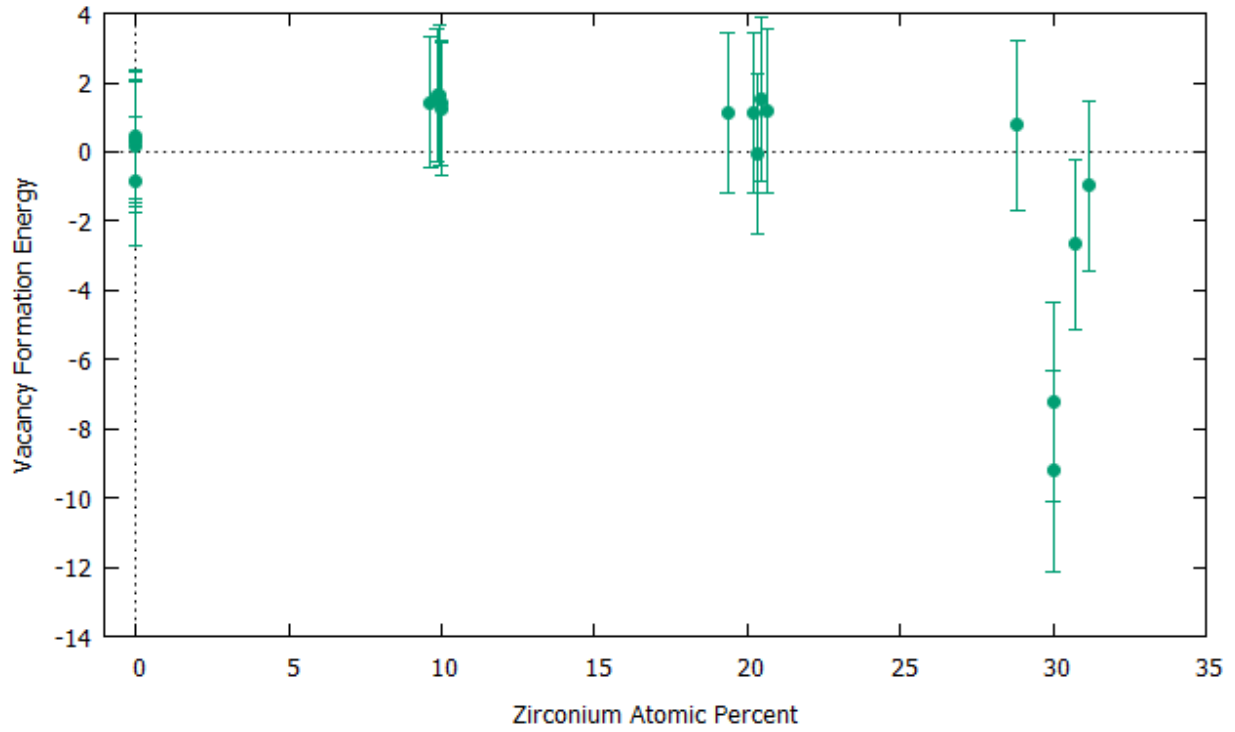Figure 21: Vacancy Formation Energy vs. Zirconium Atomic Percent for 400 K

39

Figure 22: Vacancy Formation Energy vs. Zirconium Atomic Percent for 500 K
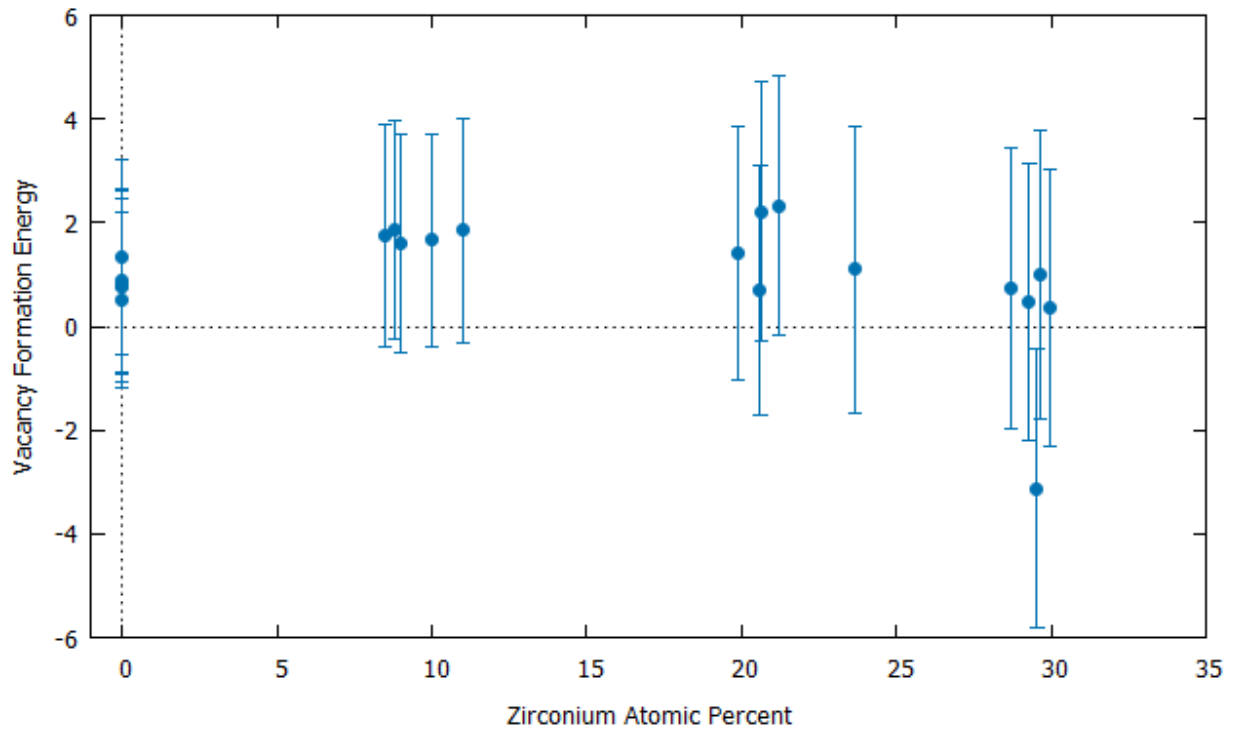

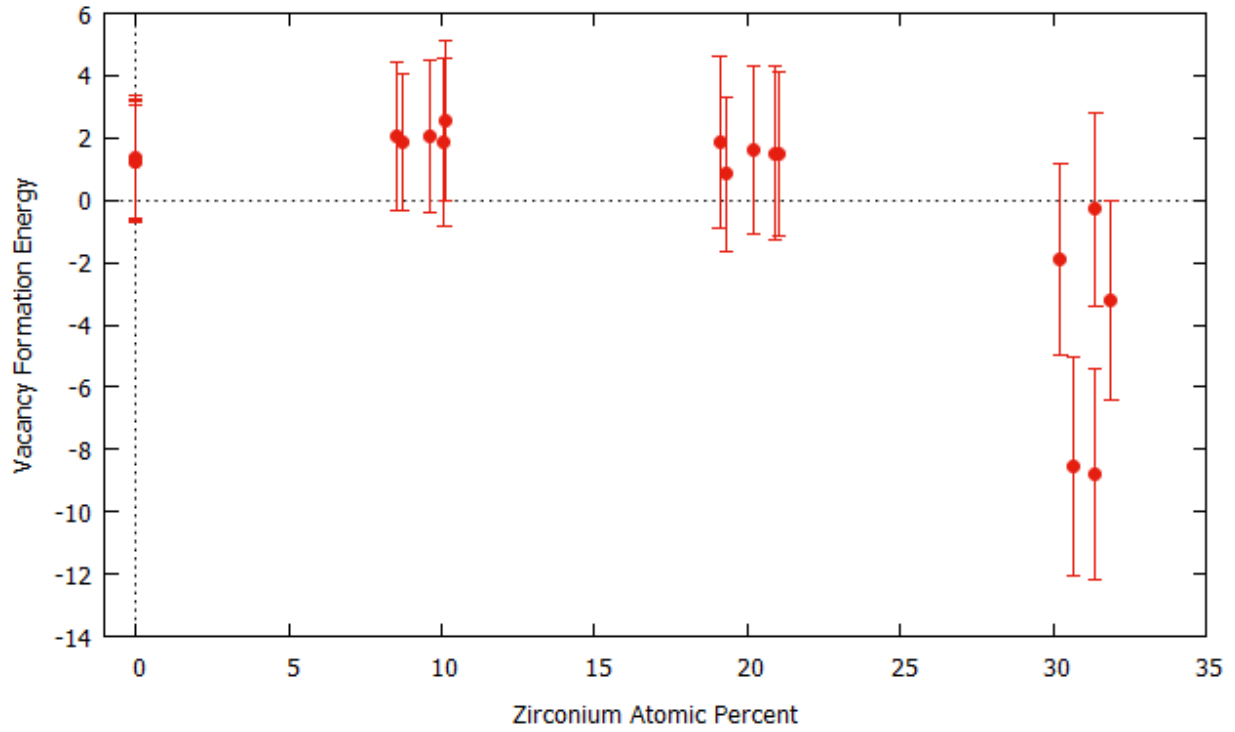Figure 23: Vacancy Formation Energy vs. Zirconium Atomic Percent for 600 K

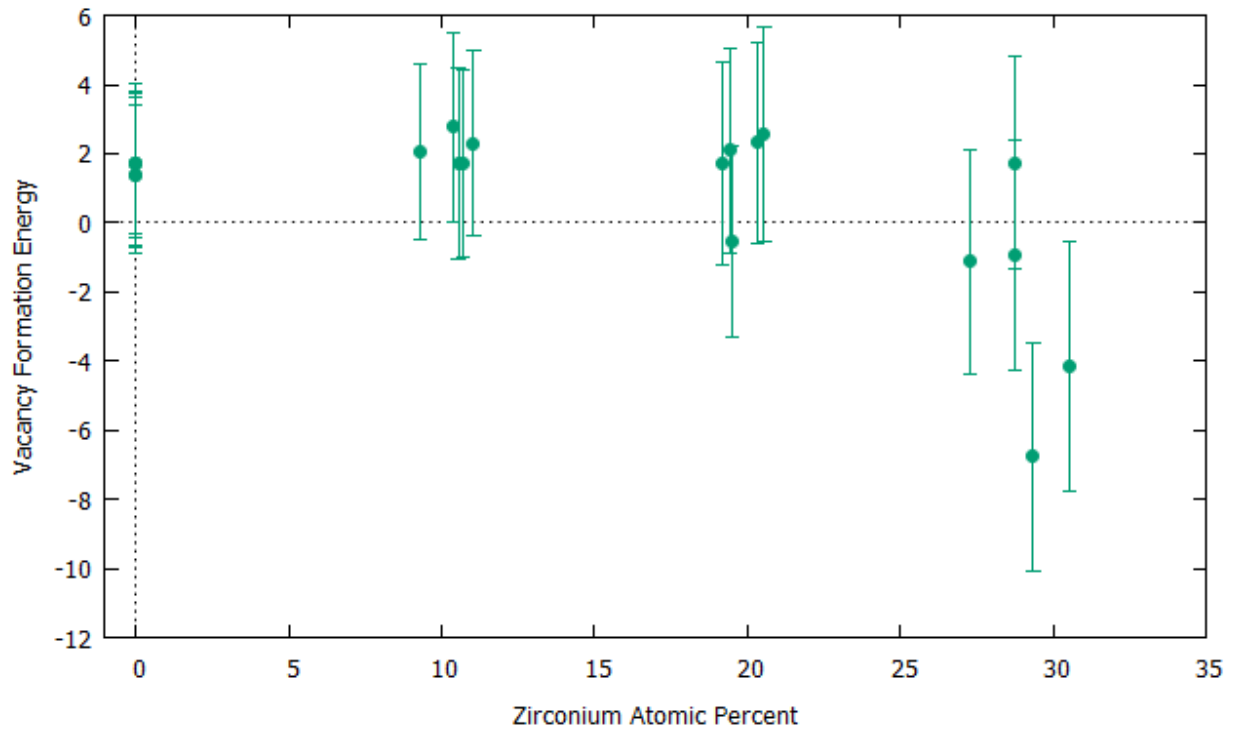Figure 24: Vacancy Formation Energy vs. Zirconium Atomic Percent for 700 K

Figure 25: Vacancy Formation Energy vs. Zirconium Atomic Percent for 800 K
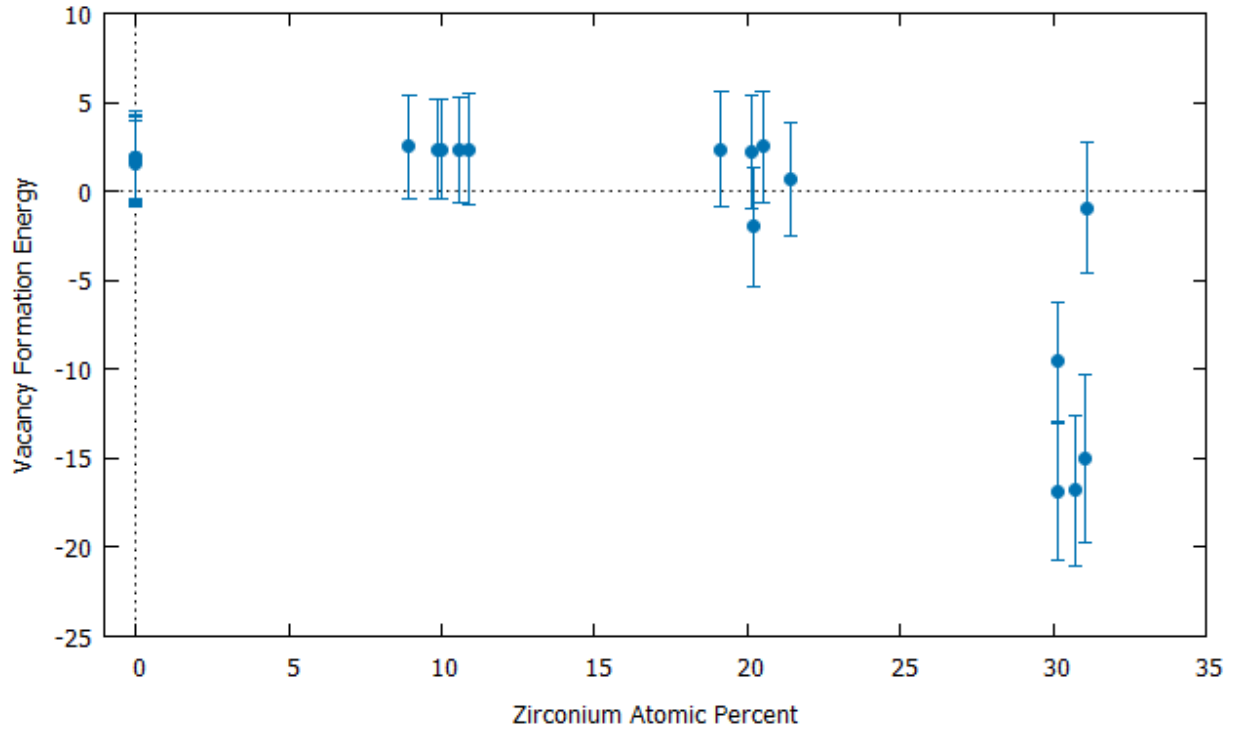
Figure 26: Vacancy Formation Energy vs. Zirconium Atomic Percent for 900 K
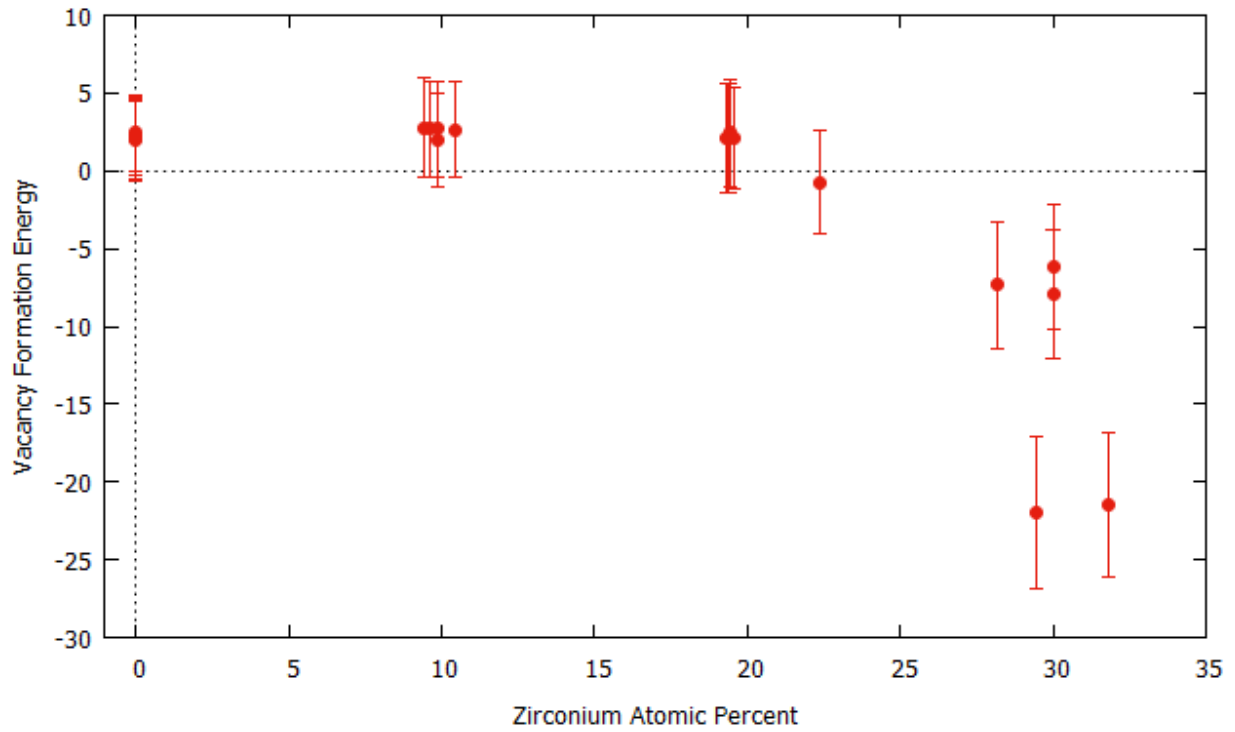

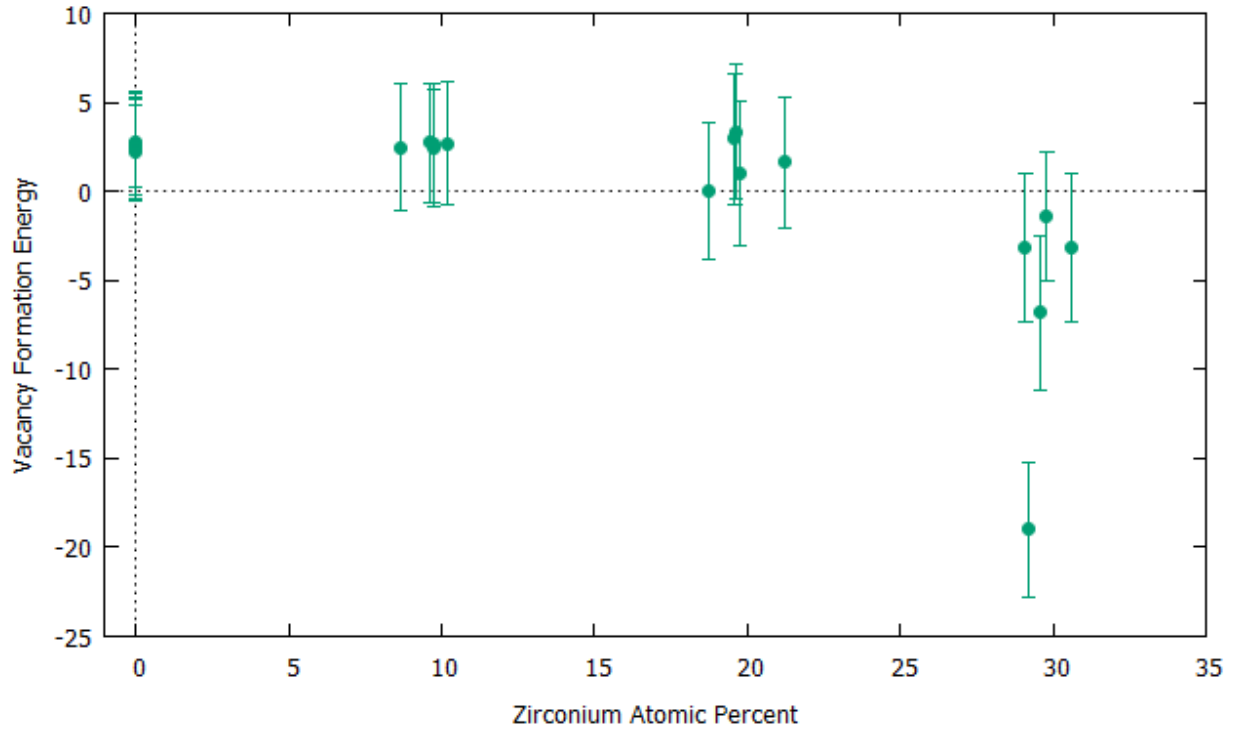Figure 27: Vacancy Formation Energy vs. Zirconium Atomic Percent for 1000 K

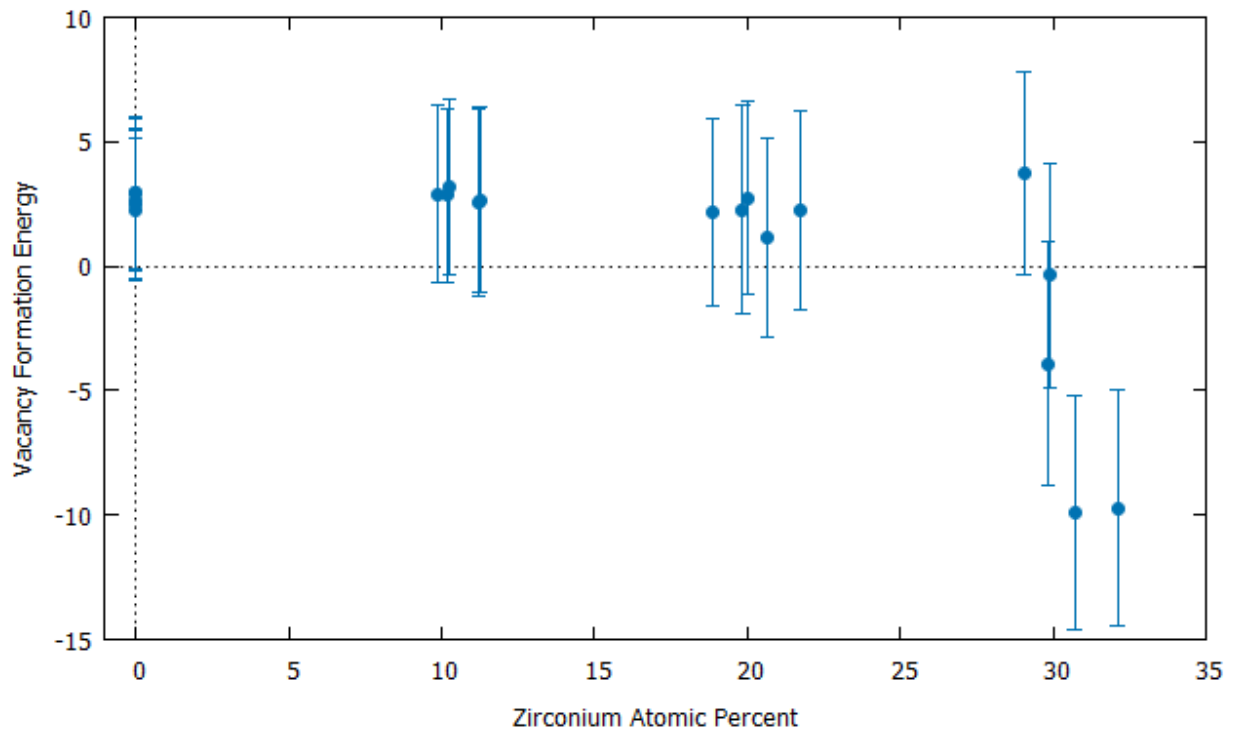Figure 28: Vacancy Formation Energy vs. Zirconium Atomic Percent for 1100 K

Figure 29: Vacancy Formation Energy vs. Zirconium Atomic Percent for 1200 K
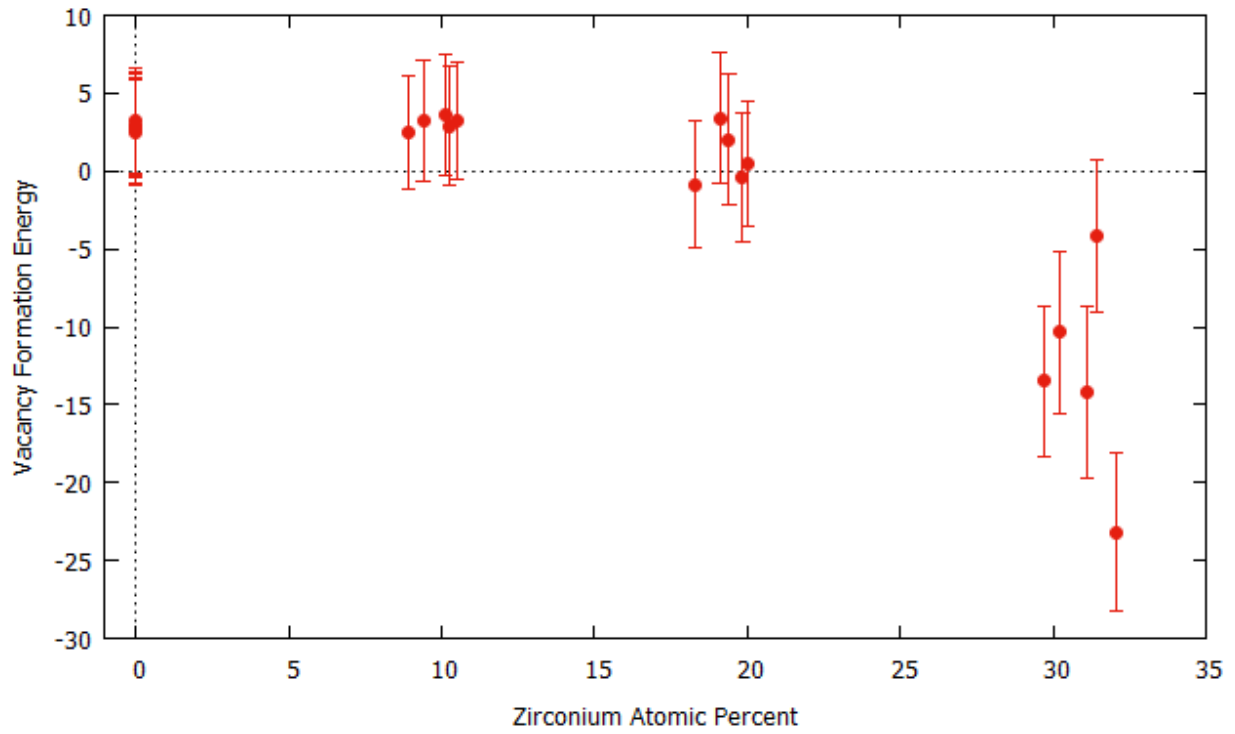
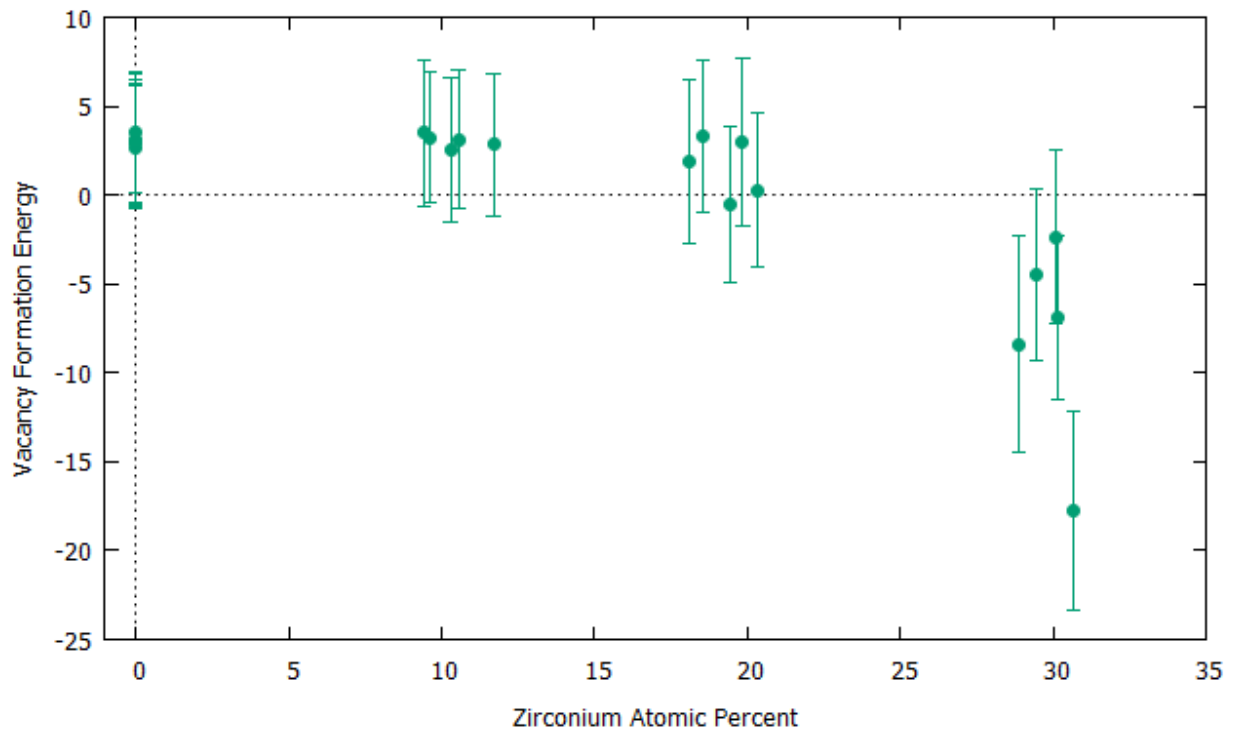Figure 30: Vacancy Formation Energy vs. Zirconium Atomic Percent for 1300 K

Figure 31: Vacancy Formation Energy vs. Zirconium Atomic Percent for 1400 K

Figures 18-31 show the results of Figures 14-17 but keep the temperature as a static variable for each figure while the percent of alloying is the independent variable. These figures also show the vacancy formation energy calculated by each individual run instead of their average, which allows the random alloying to be shown. In other words, each cluster in these figures represents either the pure uranium, 10%, 20%, and 30% zirconium, but also shows how the random alloying centered around.

The actual percentage of zirconium in each cluster does not seem to have much effect on the vacancy formation energy itself, as each cluster oscillates back in forth in terms of the vacancy formation energy. It is obvious though that a significant change in alloying from cluster to cluster does lead to significant changes in the results. The early figures show that low temperatures cause the structures to have negative vacancy formation energies across the board. As the temperatures rise, vacancy formation energies also rise, except for 30%-Zr, which due to vacancy-interstitial pairs, never has vacancy formation energies comparable to those found in the literature. If it were possible to just stop these pairs from forming, one would assume the vacancy formation energy would be at least on the order of magnitude of the other results.

Nearest Neighbors

Because the material being examined is an alloy, there is a significant chance that the composition of the nearest neighbors to the atom that is removed to create the vacancy will have a strong effect on the vacancy formation energy. To look at the effect of the nearest neighbors, a structure of 30% atomic zirconium alloy was chosen as the initial structure, and the eight nearest neighbors to the vacancy were specifically set each time, going from all eight being uranium atoms one-by-one to all eight as zirconium. For all nine configurations, the rest of the atoms were exactly the same as the exact same random number seed was used for the alloying process.

In addition, the simulation was done at 0 K to reduce any possible changes in the vacancy formation energy due to thermal movement and at 1400 K, the extreme limit of the alloy before reaching the melting point. The results are shown below in Tables 8 and 9 and Figures 32 and 33.

Table 8: Short Range Order and Vacancy Formation Energy for 0 K

Number of Nearest Neighbors	Short Range Order	Vacancy Formation Energy
0U8Zr	-0.007104851	-12.64398445
1U7Zr	-0.007429467	-19.22307885
2U6Zr	-0.0083281	-20.10604145
3U5Zr	-0.007496069	-20.09233219
4U4Zr	-0.007814961	-18.35382658
5U3Zr	-0.007555205	-18.80517178
6U2Zr	-0.007871248	-17.27299004
7U1Zr	-0.007029272	-19.29089834
8U0Zr	-0.007337559	-15.72866253

Table 9: Short Range Order and Vacancy Formation Energy for 1400 K

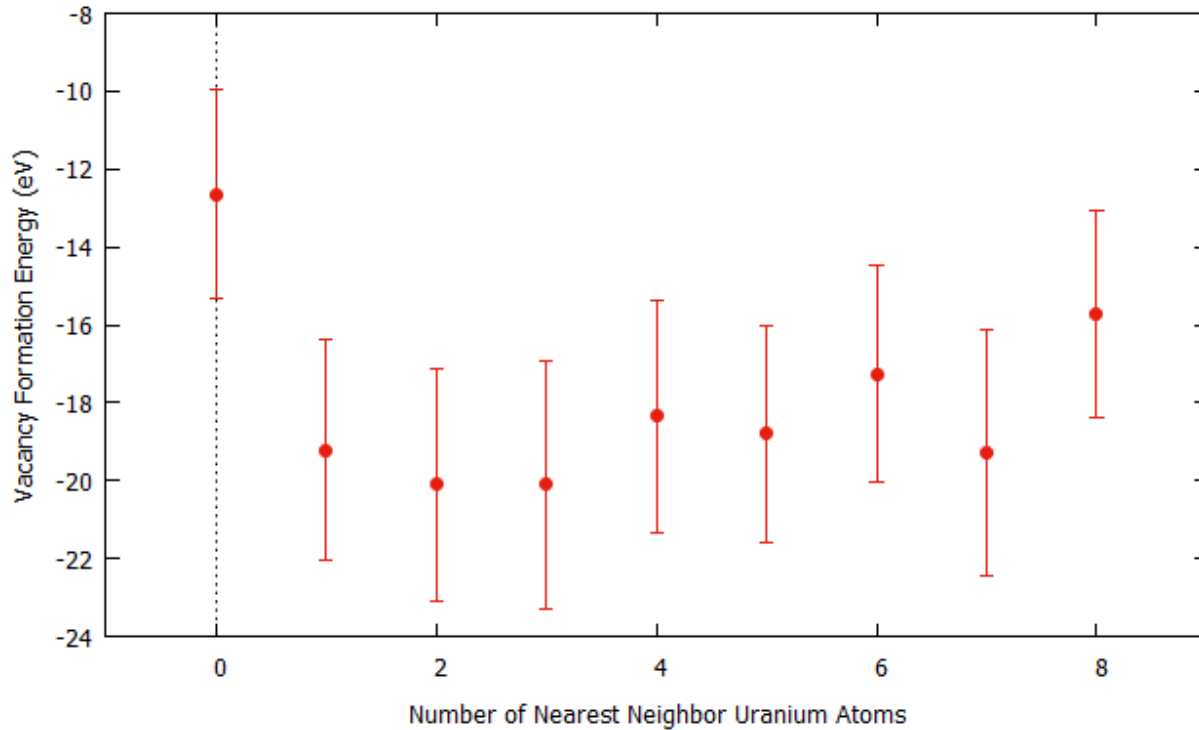| Number of Nearest Neighbors	Short Range Order	Vacancy Formation Energy
0U8Zr	-0.022303055	-25.16010849
1U7Zr	-0.020269726	-14.26362552
2U6Zr	-0.019987903	-17.54727832
3U5Zr	-0.018529887	-13.07442841
4U4Zr	-0.018822816	-13.75168474
5U3Zr	-0.017358185	-17.92938221
6U2Zr	-0.017646104	-18.34244467
7U1Zr	-0.016170732	-22.95034186
8U0Zr	-0.015867264	-10.15394285

Figure 32: Vacancy Formation Energy of 0 K as Nearest Neighbors Change

Figure 32 follows the trend of negative vacancy formation energies at very low temperatures, with an even lower vacancy formation energy than the Zr-30% alloy at 100 K. This at least indicates the trend is consistent, even if a negative vacancy formation energy does not physically make much sense. With the vacancy formation energy alternating as the nearest neighbors change, it seems that a lot more surrounding atoms affect vacancy formation energy than just the eight nearest neighbors.
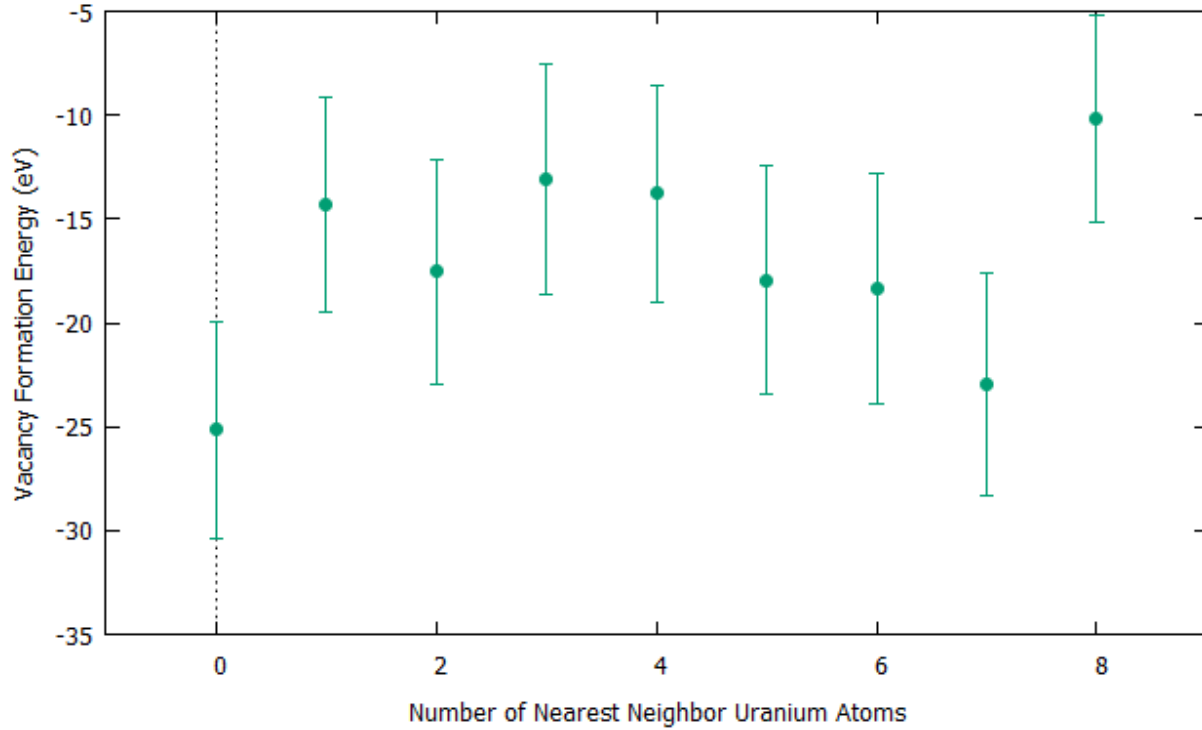
Figure 33: Vacancy Formation Energy of 1400 K as Nearest Neighbors Change

Figure 33 is similar to Figure 32 in that there is no trend in vacancy formation energy as the nearest neighbors change. Figure 33 also continues to follow the pattern of very low vacancy formation energies at higher temperatures for the 30%-Zr alloy, again due to creation of vacancy-interstitial pairs. As can be seen in both figures, the nearest neighbors of the vacancy do not seem to predict any significant pattern in the formation energy. This indicates that both uranium and zirconium provide a similar effect to the vacancy. It also may imply that vacancy formation energy is influenced heavily by atoms that do not make up the nearest neighbors.

The Short Range Order parameter gives an idea of how uniform or random a lattice of atoms is. It is calculated using equation 14 from the Methods section:

$$\sigma = -\frac{P_{AA} - n_A}{1 - n_A}$$

where P_{AA} is the fraction of nearest neighbor sites of atom type A that are occupied by A type atoms (averaged over all A type atoms) and n_A is the total atom fraction of A type atoms in the whole system.
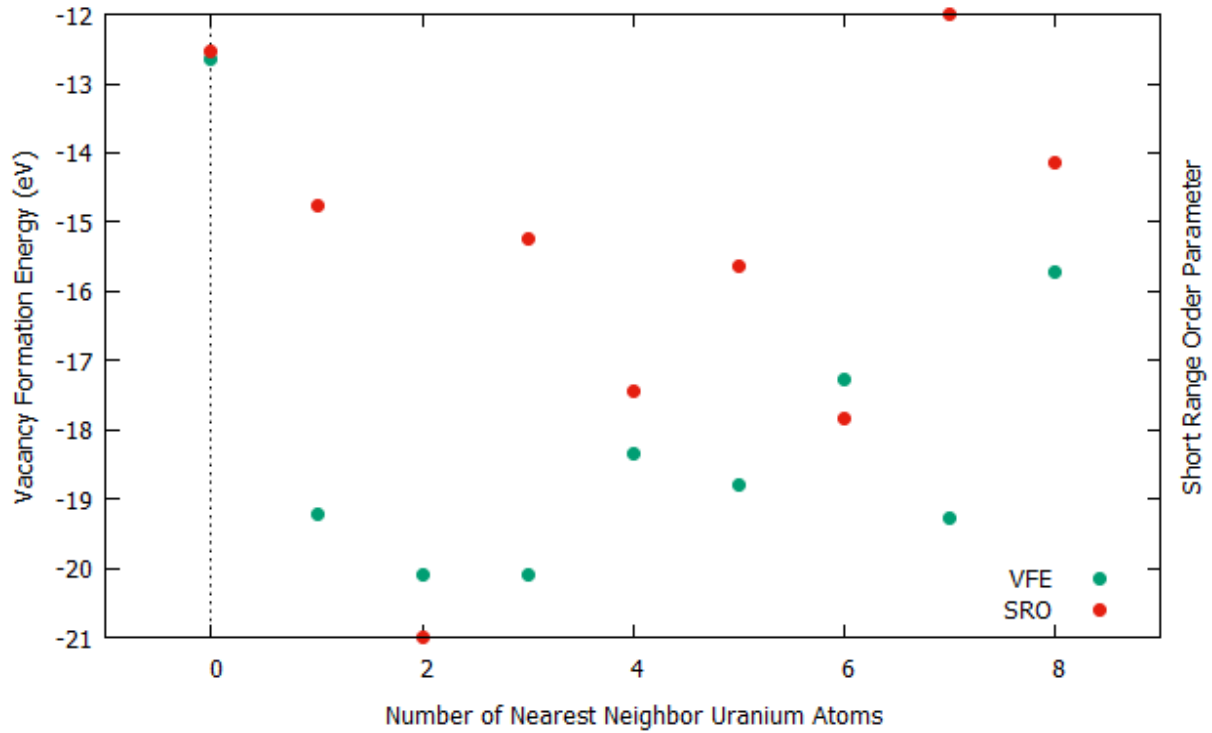

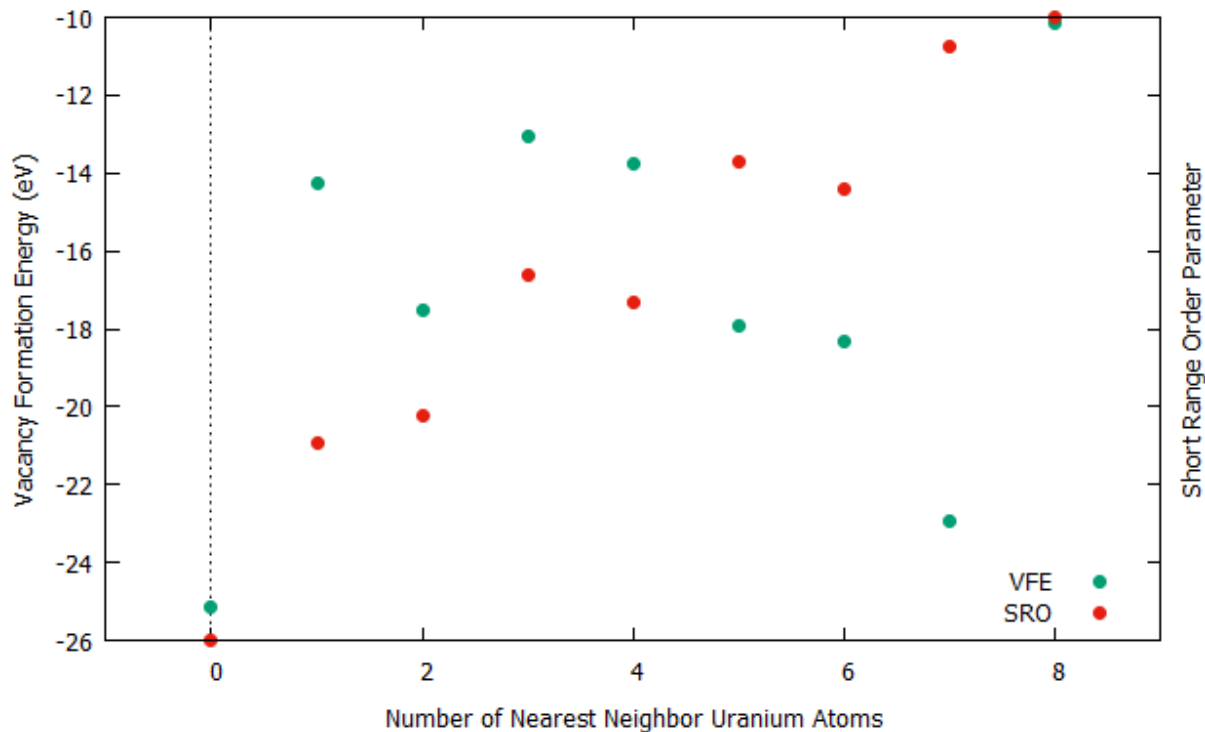Figure 34: 0 K Vacancy Formation Energy and Short Range Order Parameter

Figure 35: 1400 K Vacancy Formation Energy and Short Range Order Parameter

Looking at Tables 8 and 9 above, we see that the short range order parameters are incredibly close to zero in both temperature cases. In other words, both systems are totally random, as one would expect based on using a random process to perform the alloying. It's also of vital importance to see if the short range order seems to follow a similar pattern to the vacancy formation energy, potentially showing a more complex link between nearest neighbors and the vacancy formation energy. However, Figures 34 and 35 both refute this, both showing the short range order parameter and vacancy formation energy seeming to jump around randomly, with no discernible relation between the two.

Wigner-Seitz Defect Analysis

As previously mentioned above, vacancy-interstitial pairs have a very significant effect on the vacancy formation energy calculated through use of the simulation. These pairs increase the energy of the perfect lattice more than the lattice with the vacancy introduced due to the fact

that there are more vacancies for the interstitial to find and remove the pair in the latter case. As one could assume, this effect is more profound as the temperature of the simulation is increased, since the movement of the particles is increased as the temperature increases and therefore more likely to end up in another lattice position. However, this effect is also notable when the atomic percentage of zirconium increases. This could be due to the fact that the atomic lattice was initialized using uranium lattice constants, and once zirconium atoms are placed instead, the incorrect lattice constants allow more vacancy-interstitial pairs to be created.

Wigner-Seitz defect analysis works by taking a reference lattice, which is the original perfectly-structured lattice in the simulation before it is allowed to run, and comparing it to the lattice at each timestep. The analysis finds a vacancy if there is not an atom near where the reference lattice had an atom and it marks an interstitial if there are two or more atoms near where the reference lattice had an atom.
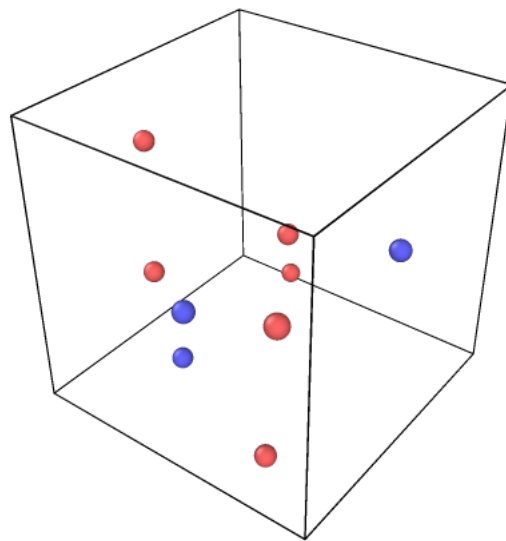

Figure 36: Vacancies and Interstitials During Final Step of U-30%Zr at 1200 K (Red and Blue are Uranium and Zirconium Starting Positions, Respectively)

Figure 36 gives an example of Wigner-Seitz defect analysis by showing one timestep's defects. There are nine spheres, indicating nine defects. One defect is the vacancy intentionally introduced in the lattice while the other eight are vacancy-interstitial pairs formed naturally during the simulation.
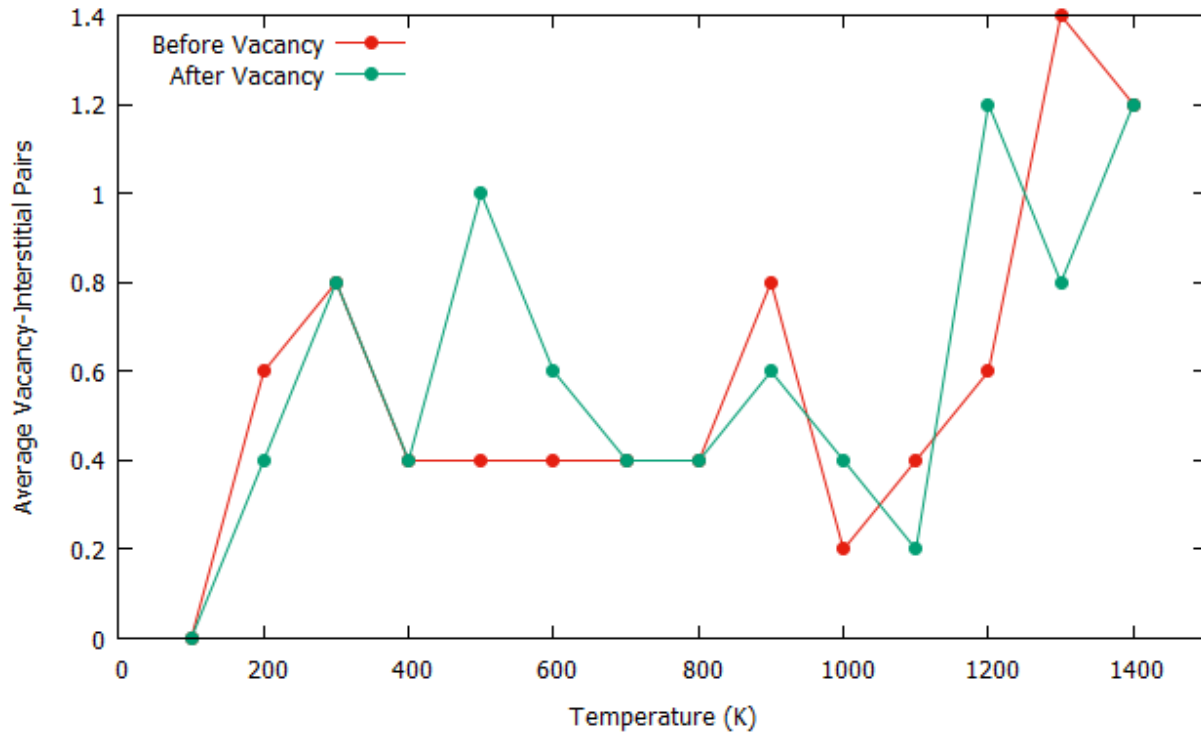

Figure 37: Average Number of Vacancy-Interstitial Pairs vs. Temperature for Zr-20%
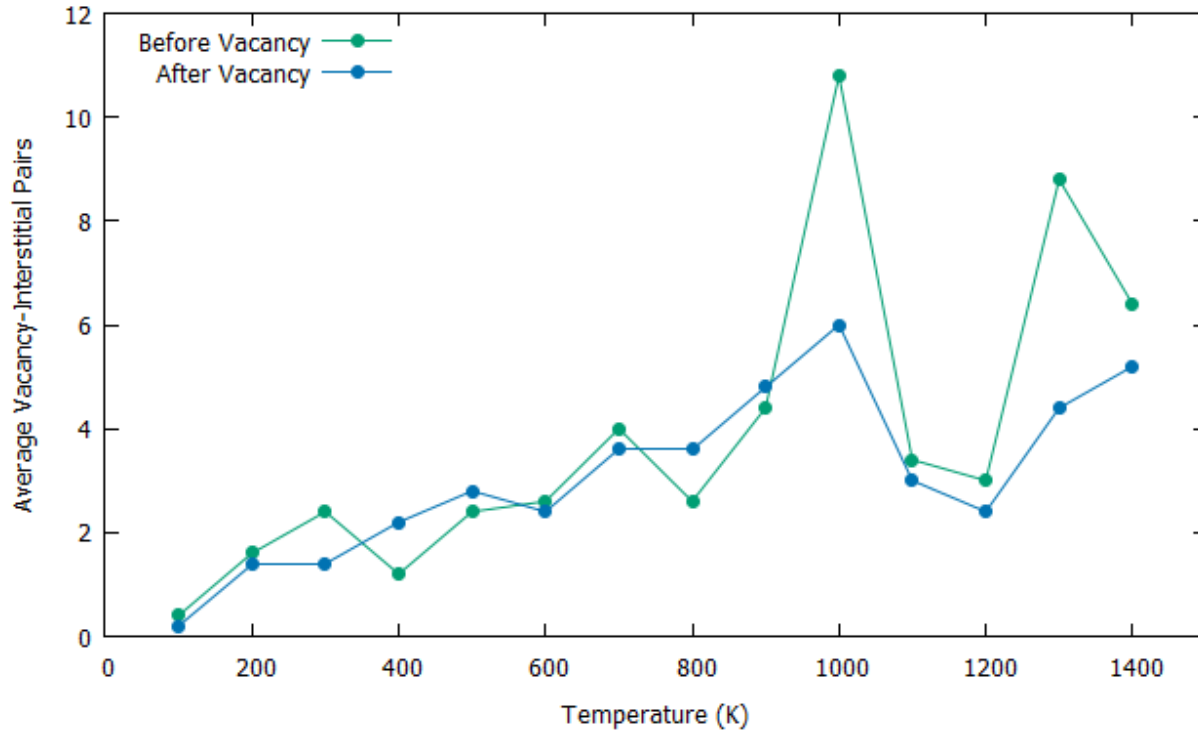
Figure 38: Average Number of Vacancy Interstitial Pairs vs. Temperature for Zr-30%

It should be mentioned that Figures 37 and 38 were created using the number of vacancy-interstitial pairs at the end of each portion of the run and then averaging all five runs of temperature and atomic percentage conditions in order to make each data point. While this misses out on times when there are more vacancy-interstitial pairs in the middle of the run, it does a good job of showing the general trend of more vacancy-interstitial pairs as the temperature increases and as the atomic-percentage of zirconium increases. The pure uranium cases and the Zr-10% cases were not included because there was only one single case that ended with a vacancy-interstitial pair. Despite this, there were several simulations where vacancy-interstitial pairs were created during the runs but had rejoined before the simulation was done.

It's also interesting to note that both Zr-20% and Zr-30% experience a drop in the number of defect pairs around 1000 K, which is the temperature at which the BCC γ-uranium and β-zirconium allotropes actually begin to form. It seems that once the simulations are being

run at realistic temperatures for the BCC-phases to exist, the likelihood of vacancy-interstitial pairs being created decreases. However, the increased energy due to higher temperatures still leads to more defect pairs, especially as the melting point of the alloy is almost reached.

Common Neighbor Analysis

Common Neighbor Analysis is used to ensure that the alloy remains in the BCC phase throughout the simulation by using an algorithm to analyze the local atoms and determine which part of the structure is in which phase. Similar to the formation of vacancy-interstitial pairs, the percentage of the structure that remains in the BCC phases decreases as both temperature and the atomic-percentage of zirconium increase.
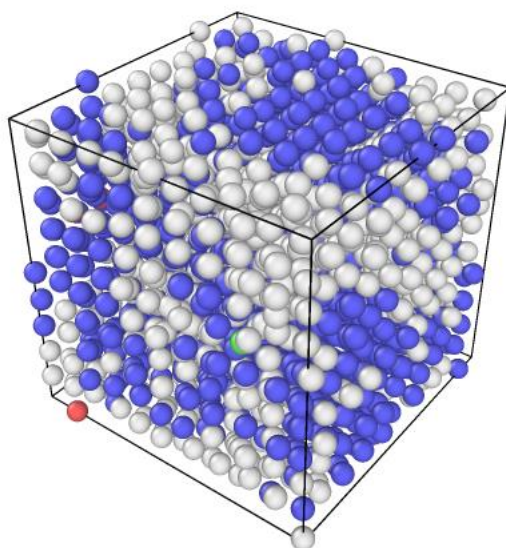
Figure 39: Common Neighbor Analysis of U-30%Zr at 1200 K (Blue = BCC, Green = FCC, Red = HCP, Gray = Other)

Figure 39 gives an example of what common neighbor analysis looks like. As can be seen, a significant portion of the structure is still in the BCC phase while another huge part cannot be classified as a phase at all by the algorithm, due to the atoms' vibrations due to the temperature and random defect pairs being produced. There are also a few FCC and HCP atoms,

which are more than likely simply random arrangements that happen to look like FCC and HCP
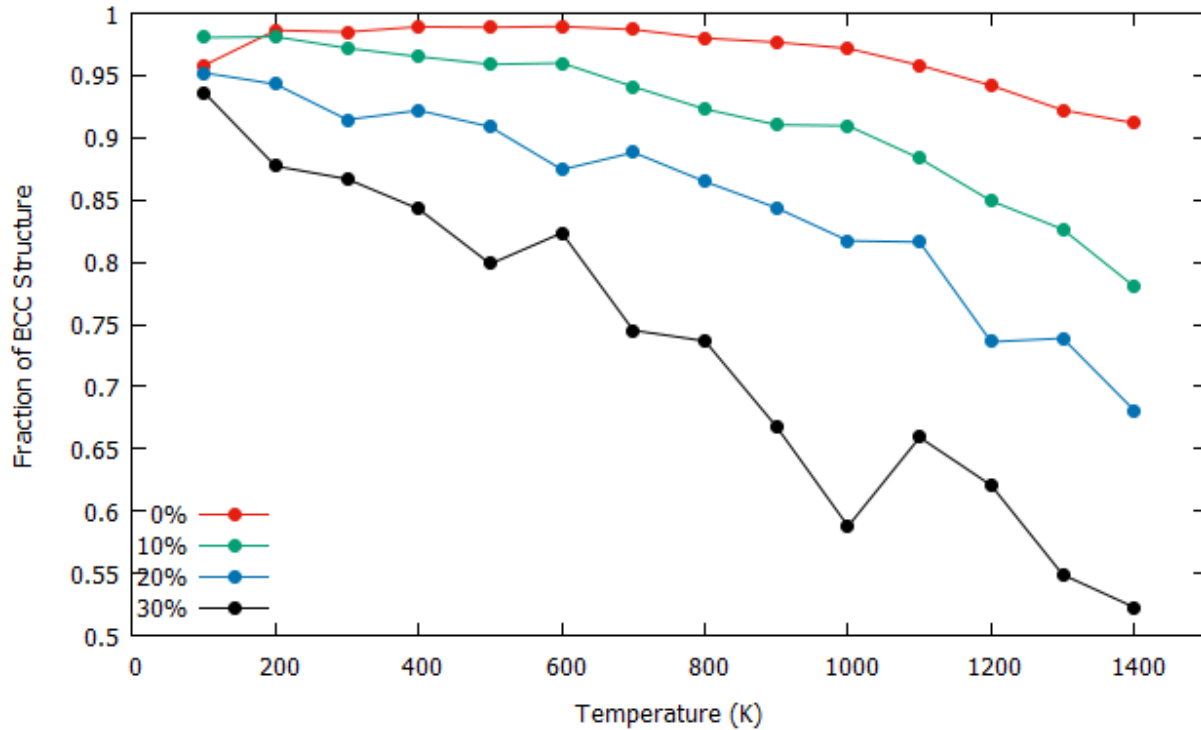
to the algorithm.

Figure 40: Fraction of Simulation in BCC Phase vs. Temperature

Figure 40 shows the decrease in BCC structure for the four different alloys as

temperature increases. This decrease is much more obvious as the percentage of zirconium

increases, with Zr-30% nearly reaching less than 50% BCC phase. It's also worth noting that, as

in the vacancy-interstitial pair formation, there is a break in the pattern after 1000 K. The Zr-20%

simulations seem to level out in the decreasing BCC fraction, while Zr-30% actually jumps back

up. After this point, all of the conditions have a much more quickly decreasing BCC fraction,

which can be seen more obviously in Figure 41 below, focusing solely on the pure uranium case.

Again, it seems likely that this is due to the fact that the phases being studied actually exist in

reality around 1000 K.

Interestingly, the pure uranium simulations experience a brief increase before actually decreasing around 600 K. As previously discussed, this initial increase could be due to the fact that all of the lattice constants properly apply to all of the atoms in the simulation, allowing the simulations to retain their structure before the increased temperature imparts enough energy to lead to a bit of a break down of the BCC structure, as shown zoomed in in Figure 41.
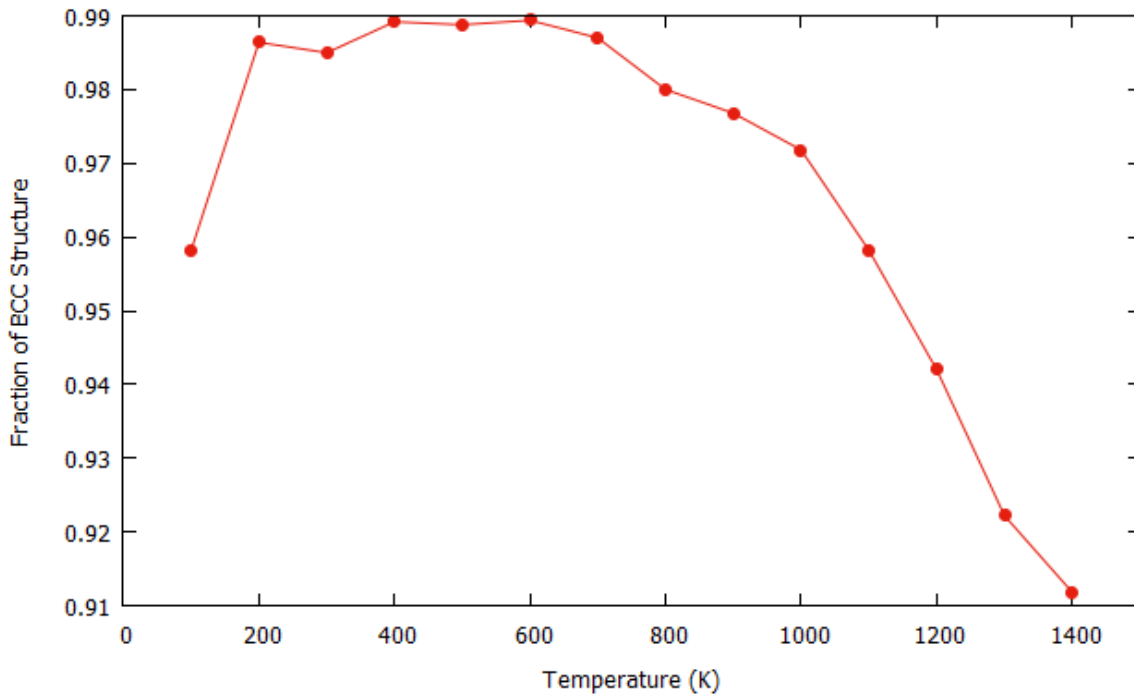

Figure 41: Fraction of Simulation in BCC Phase vs. Temperature for Pure Uranium

Radial Distribution Function

The Radial Pair Distribution Function measures the probability of finding a particle within a certain distance of any other particle. When plotted, the function tends to peak around the lattice constant, as one would expect. Unsurprisingly, the function tends to grow wider around the peak as temperature and atomic percentage of zirconium increases. Figures 42 through 53 below show select snapshots in order to illustrate this.

Figure 42: Radial Distribution Function for Zr-00% and 200 K

Figure 43: Radial Distribution Function for Zr-00% and 800 K

Figure 44: Radial Distribution Function for Zr-00% and 1300 K

Figure 45: Radial Distribution Function for Zr-10% and 200 K

Figure 46: Radial Distribution Function for Zr-10% and 800 K

Figure 47: Radial Distribution Function for Zr-10% and 1300 K

Figure 48: Radial Distribution Function for Zr-20% and 200 K
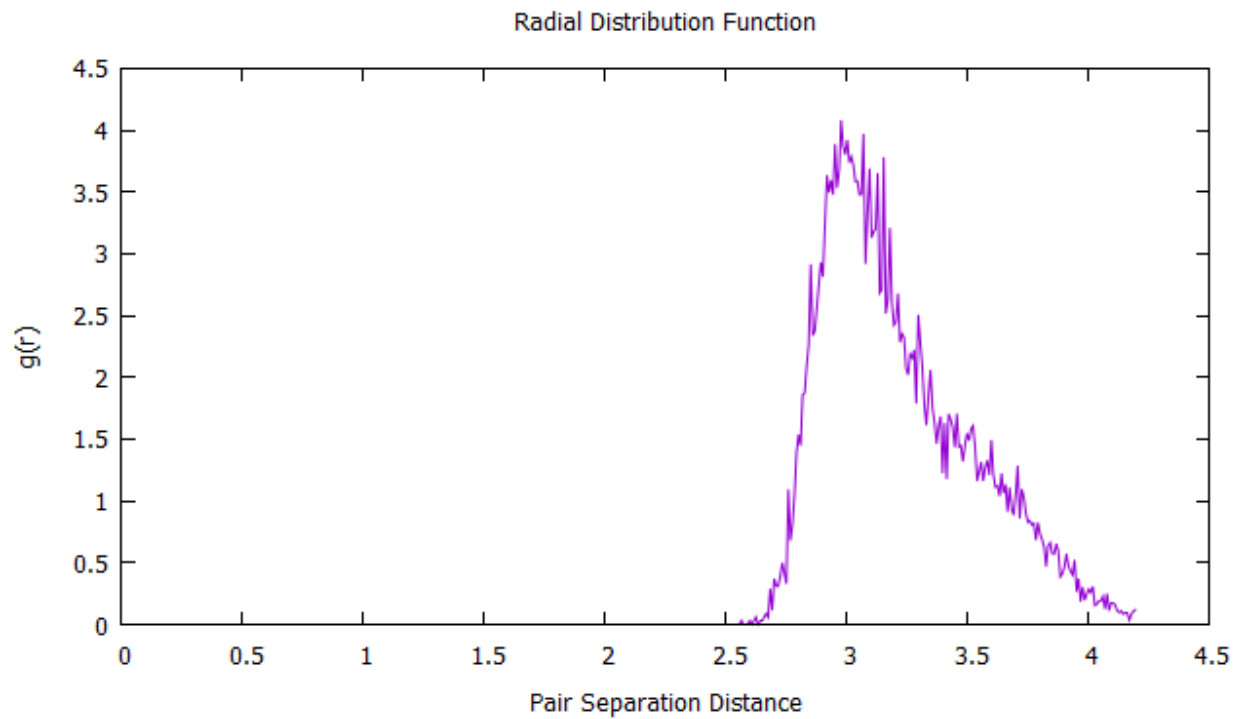
Figure 49: Radial Distribution Function for Zr-20% and 800 K
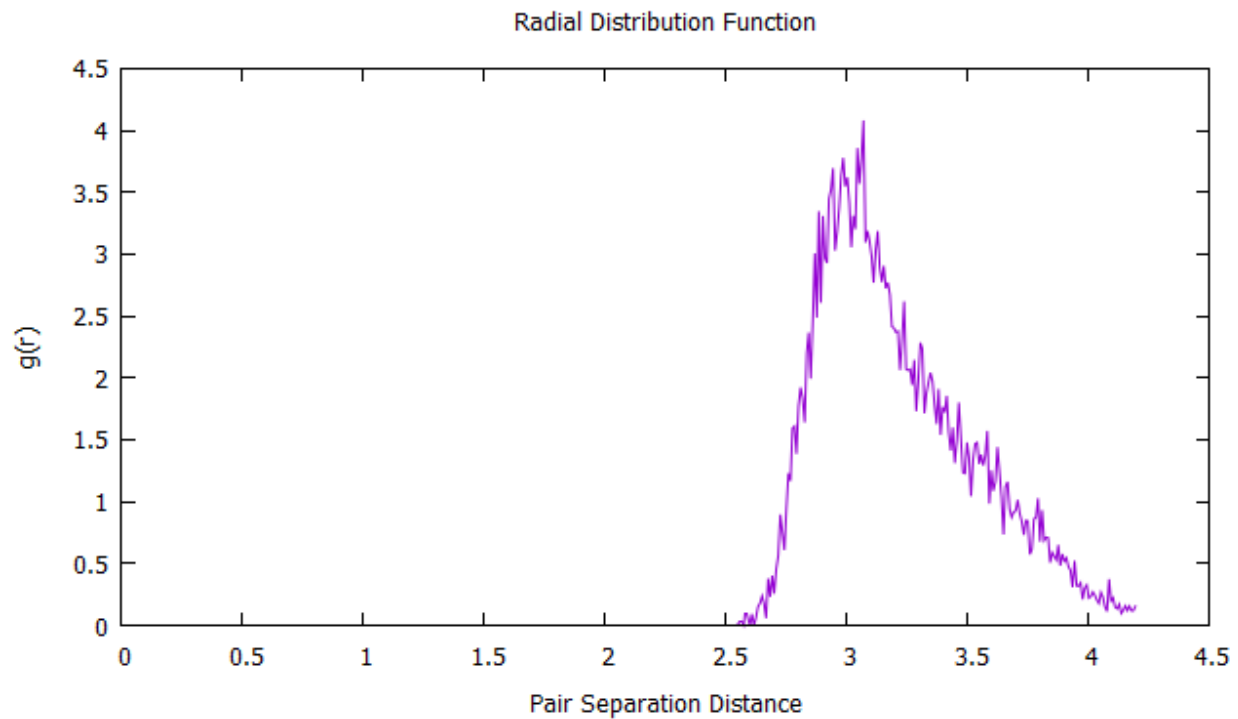
Figure 50: Radial Distribution Function for Zr-20% and 1300 K
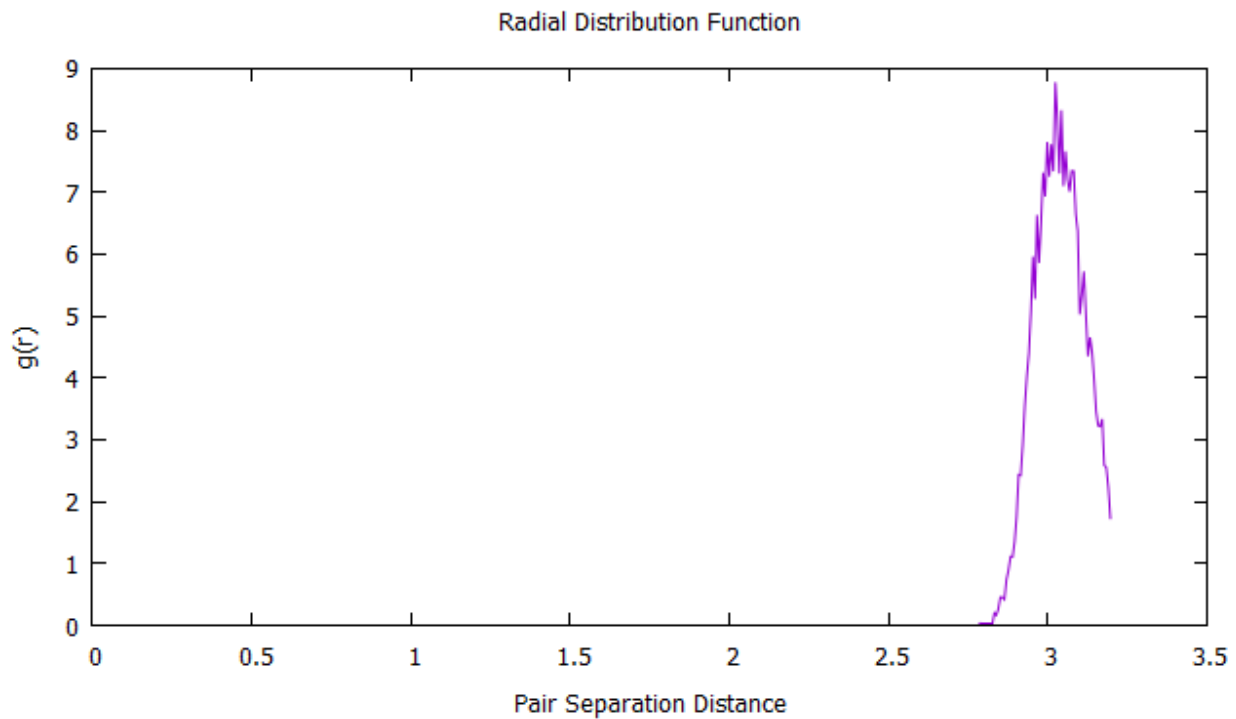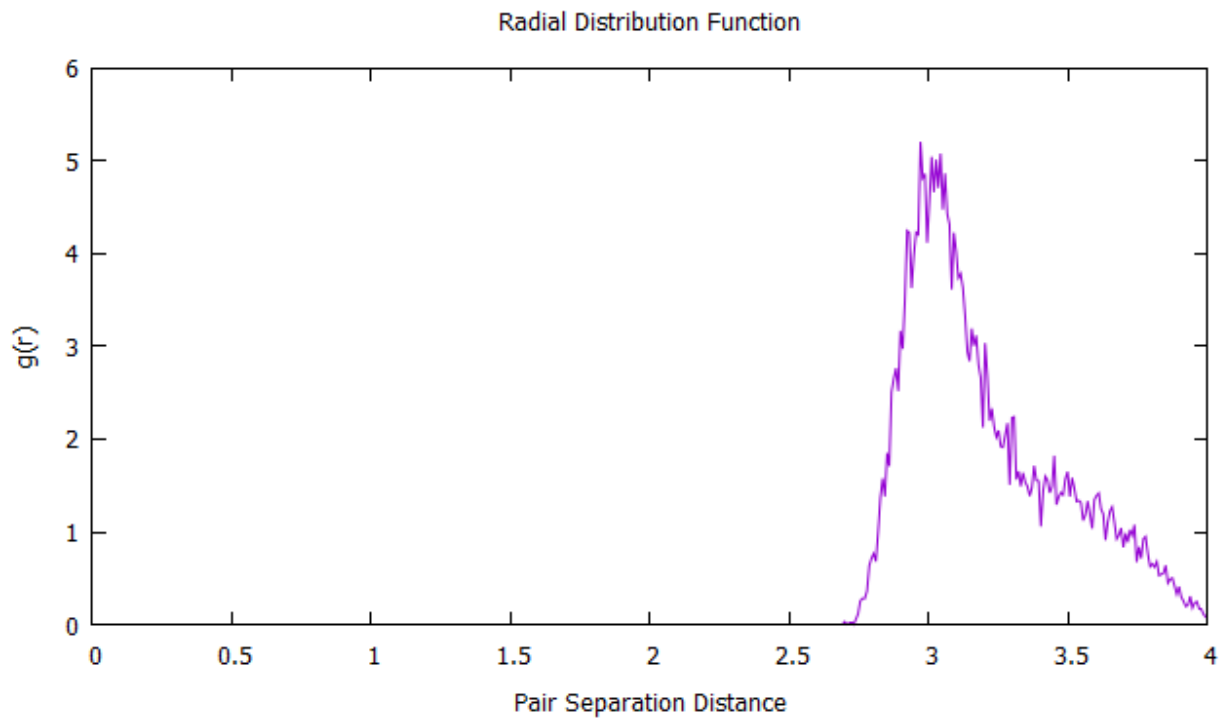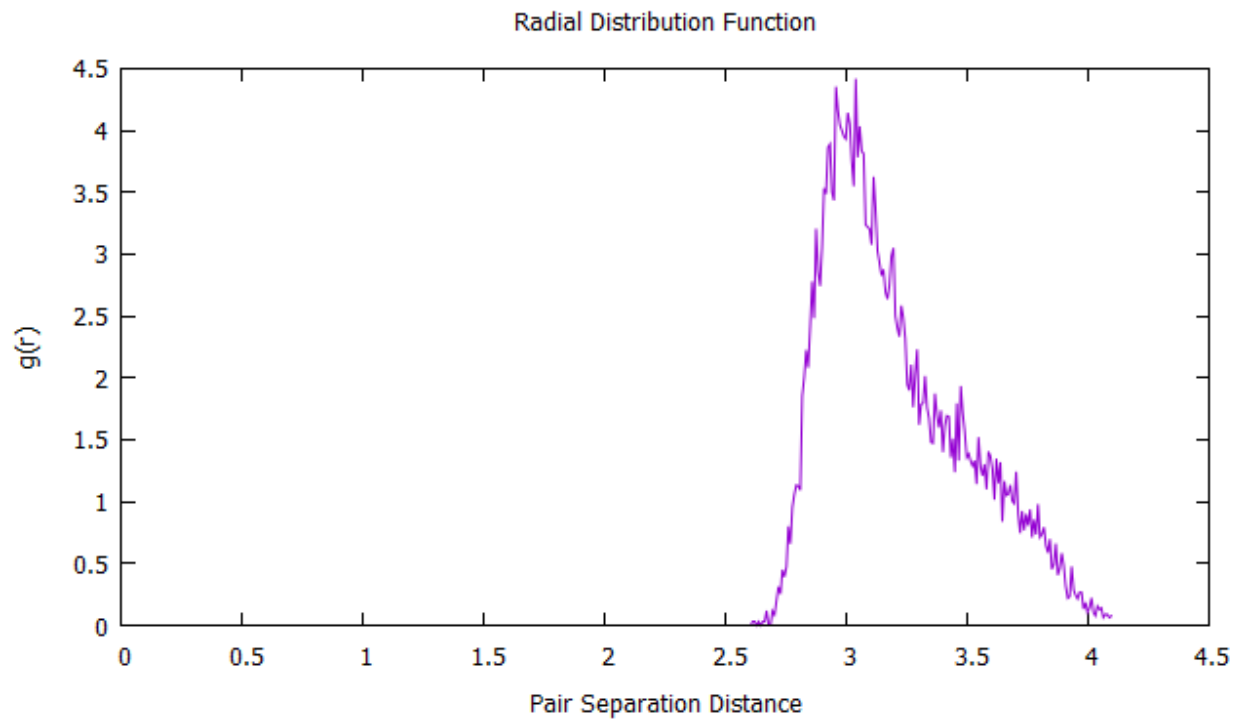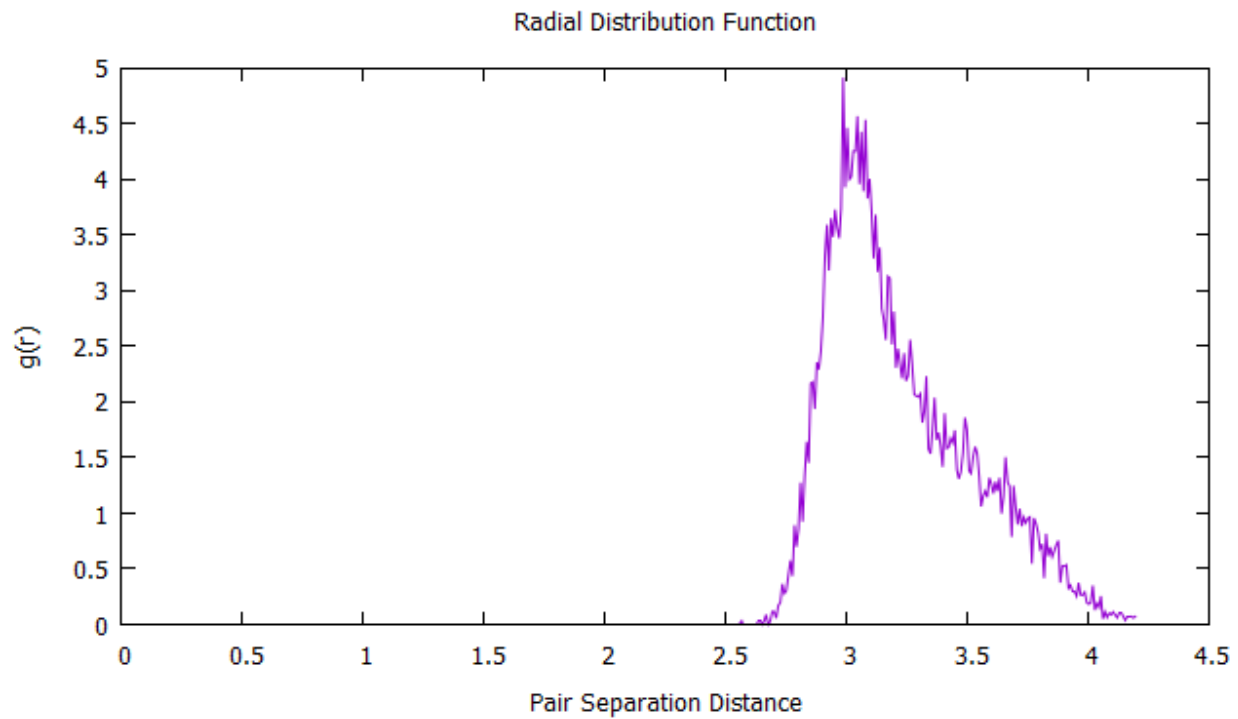

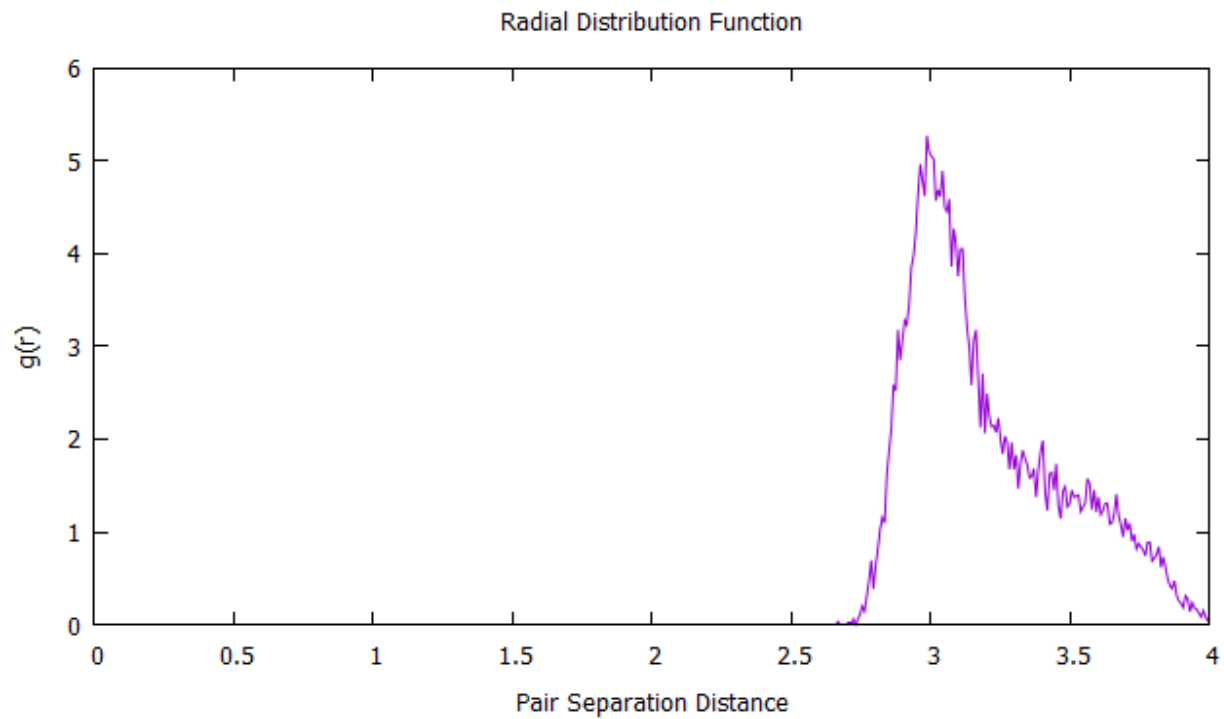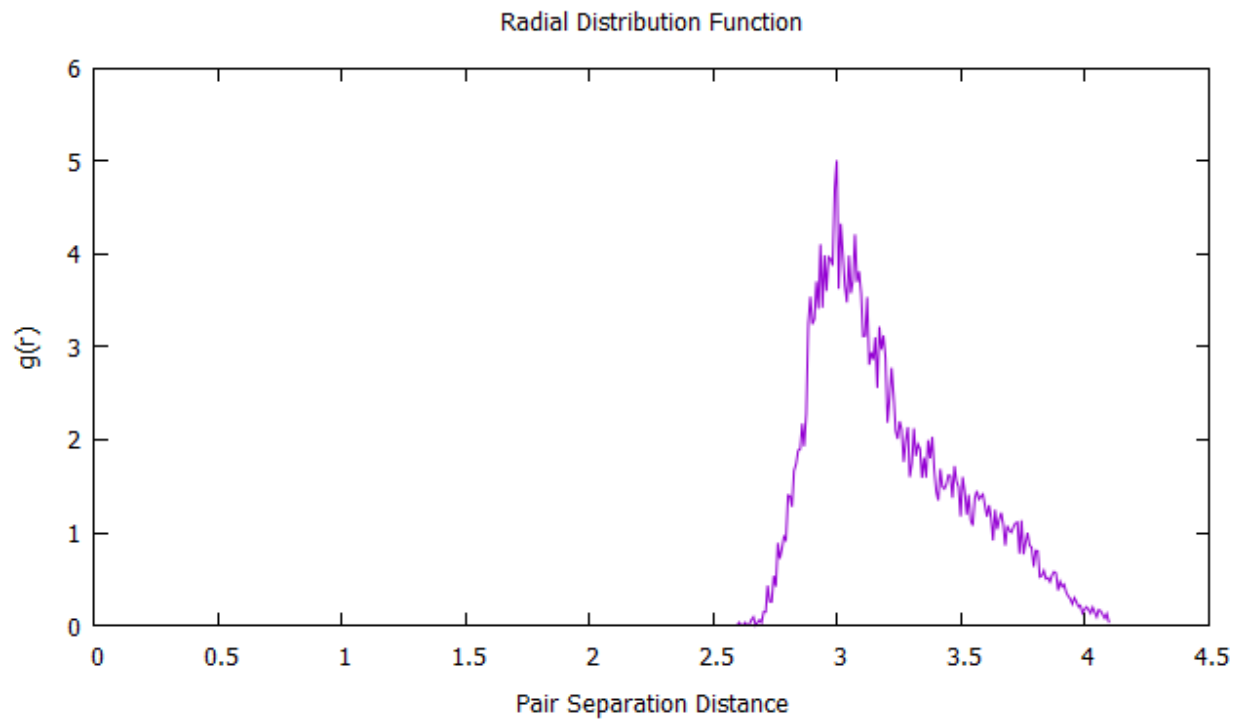Figure 51: Radial Distribution Function for Zr-30% and 200 K

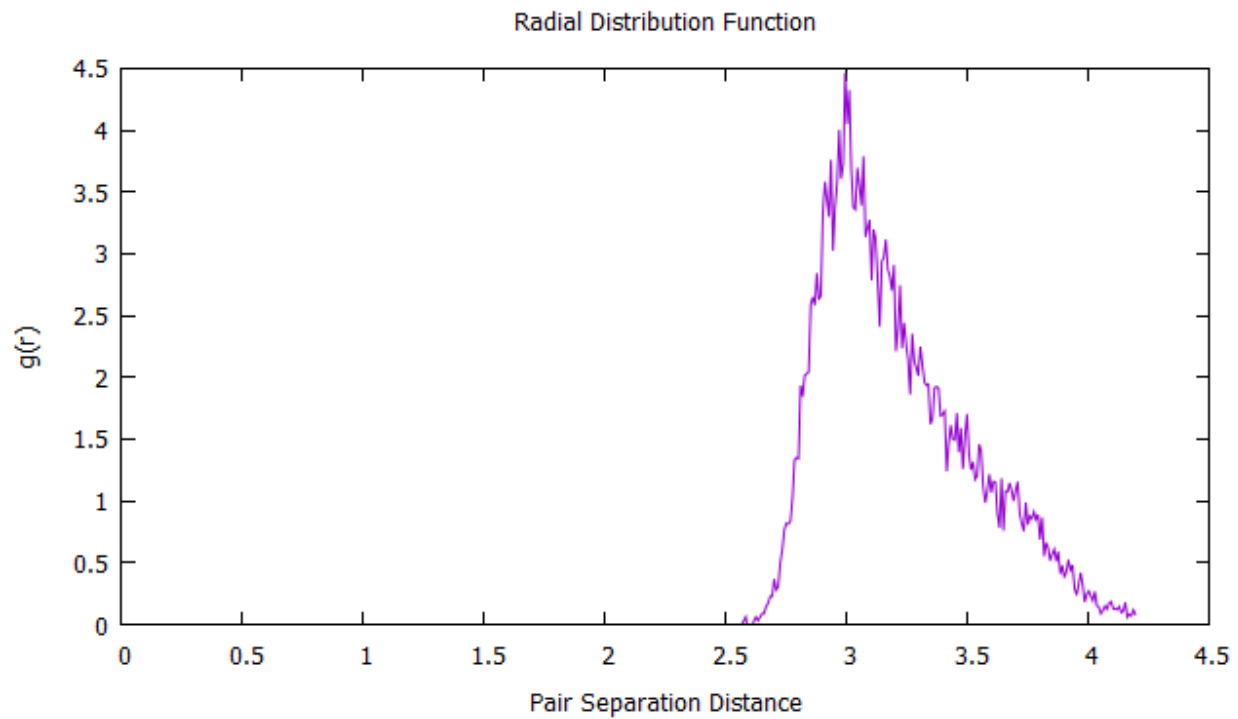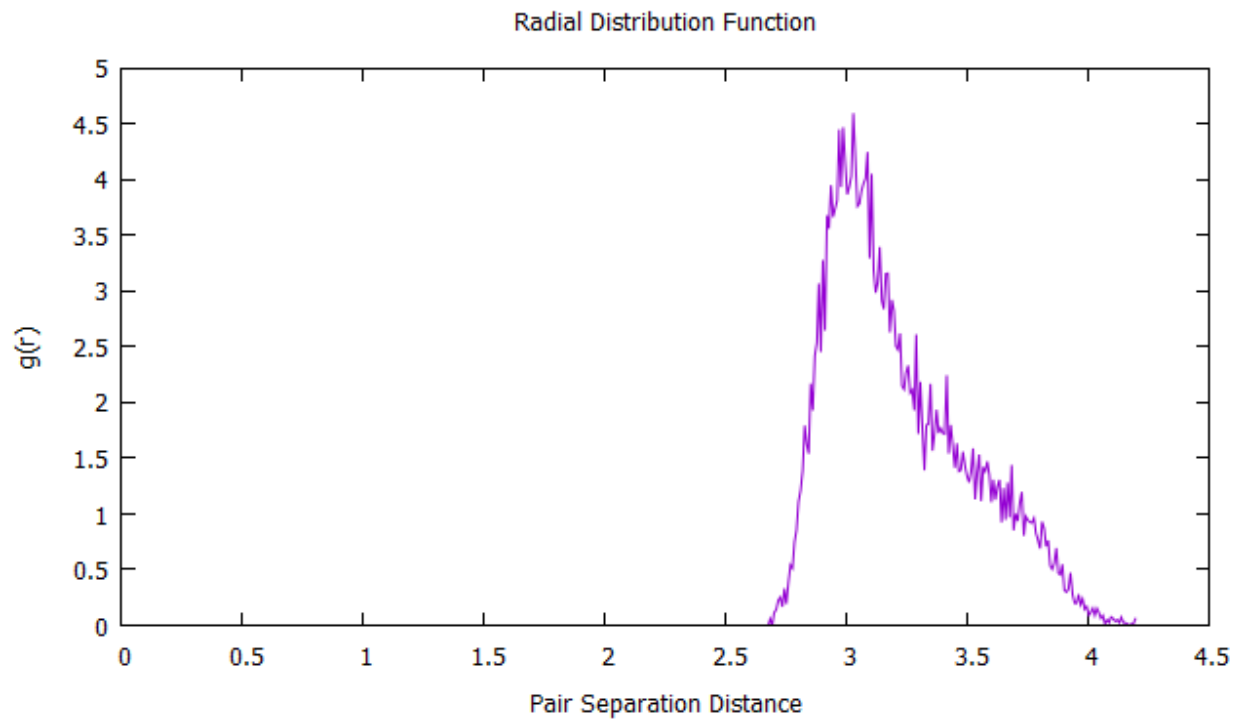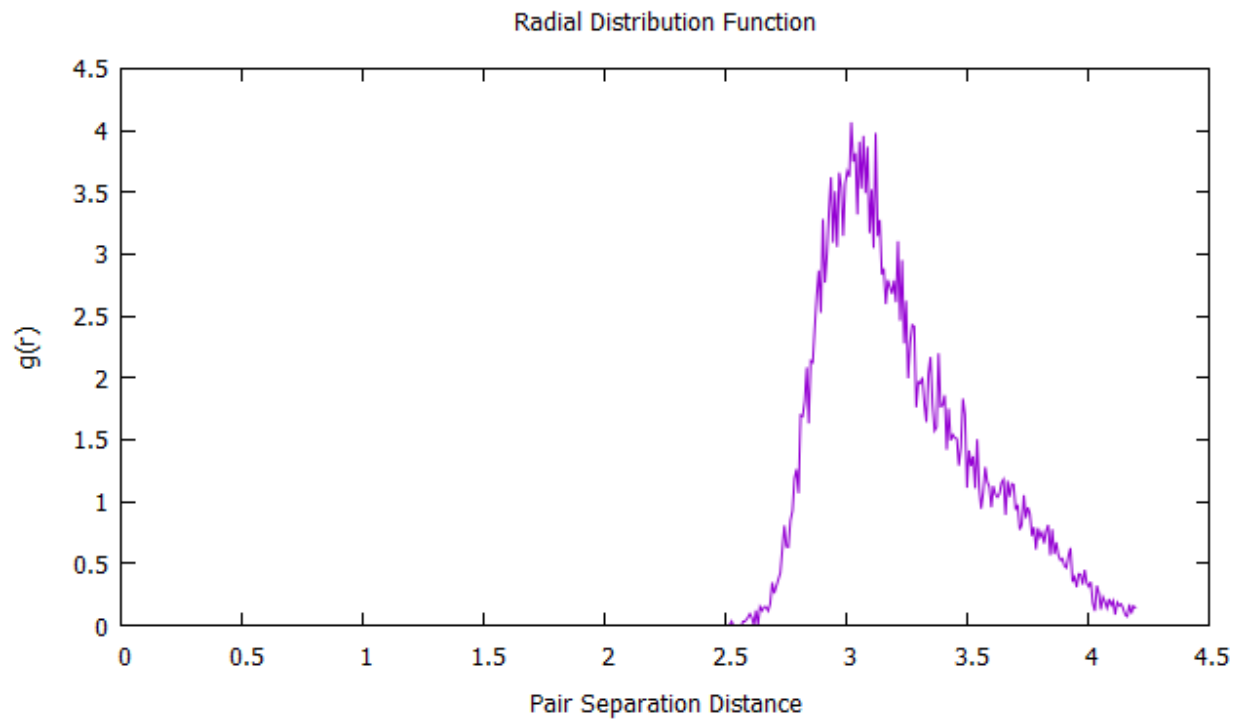Figure 52: Radial Distribution Function for Zr-30% and 800 K
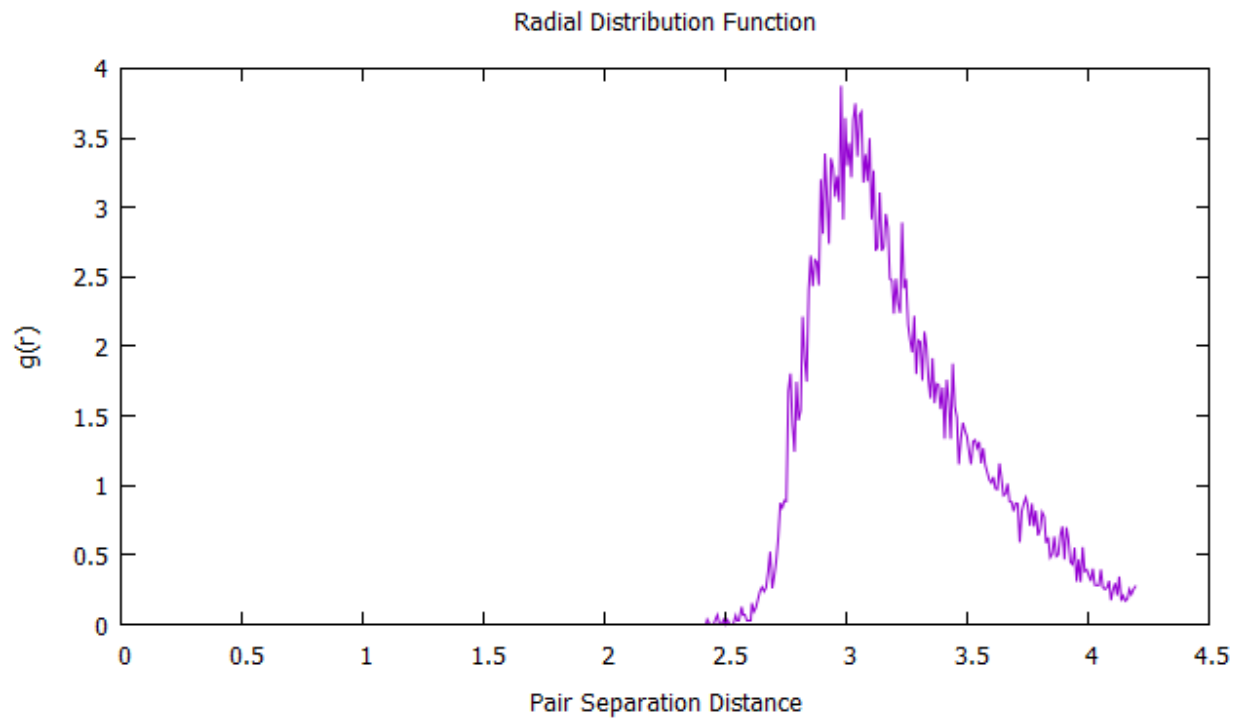
Figure 53: Radial Distribution Function for Zr-30% and 1300 K

Figures 42 – 53 show the general trends previously described in common neighbor analysis but by using a different analytical tool. As the amount of zirconium in the alloy goes up, we see a wider pair-separation distance distribution, attributable to the fact that the original lattice was set up using uranium lattice constants before randomly inserting the alloying zirconium. The trend of increasing temperature leading to a wider distribution in the pair separation distance is also shown, as the three radial distribution functions per alloying percentage show. The higher temperatures lead to higher energy atoms, allowing them to move further and further from their original position before the overall lattice forces push the atom back.

Only a handful of the total radial distribution functions were chosen to be shown in order to reduce the amount of space the figures took up, but the three varying temperatures for each alloy show enough of the trend, which has been shown repeatedly throughout the paper already.

Chapter 4: Conclusion

With advanced reactor designs being pushed as the future of nuclear energy, finding the best fuel materials is of vital importance. One of the top candidates for advanced reactor fuel is the uranium-zirconium alloy. Despite the alloy's potential, a lot of data, even basic properties, has not yet been investigated and published. This work utilizes the Modified Embedded-Atom Method (MEAM) interatomic potential developed by Moore to continue collecting data on the BCC uranium-zirconium alloy, since reactor operating temperatures mean the alloy will be in the BCC phase. This MEAM interatomic potential is the first interatomic potential developed for the U-Zr alloy.

This work focused mostly on the U-Zr's vacancy formation energy, and found that, under the right circumstances, the MEAM interatomic potential seemed to do a good job of simulating the correct vacancy formation energy. In particular, these conditions were ones where the simulations were run at the correct temperatures for the BCC phase to exist, and also at the lowest percentages of zirconium. The vacancy formation energies found under these conditions are close to the vacancy formation energies of pure uranium and zirconium found in the literature. This follows Moore's conclusions that his MEAM interatomic potential best described majority-zirconium alloy; however, this is not much help as the alloys used in reactors will be majority uranium. With all of this in mind, the U-20Zr alloy is recommended as the best potential candidate for advanced reactor fuel design. This alloy contains the highest amount of zirconium that did not seem to break down in Common Neighbor Analysis and did not have

anywhere near as many vacancy-interstitial pairs forming in Wigner-Seitz Defect Analysis as the U-30Zr. The highest amount of zirconium is desired because of the thermal properties in zirconium balancing out uranium's undesired thermal properties.

The vacancy formation energies that did not match predictions, however, did follow reasons found in literature for not following. First, at low temperatures, the BCC phase would not exist, so it makes sense the vacancy formation energy would often be negative. The other cases with a low or negative vacancy formation energy was predicted by the number of vacancy-interstitial pairs, which affects the energy of the perfect lattice more, leading to the negative vacancy formation energy.

Besides the vacancy formation energy, several analysis techniques were performed on the simulations, giving a better idea of how well the lattice holds its phase during the short simulation. Again, lower amounts of zirconium and being at operating temperature both had an effect on the results, being attributable both to the MEAM interatomic potential's limitations and the formation of vacancy-interstitial pairs.

The MEAM interatomic potential could definitely use more work in various scenarios, but as a first step, does a good job describing other properties very well. With how important it seems the uranium-zirconium alloy will be going forward in the future, this work is a good step in the right direction for advanced reactor fuels.

Input File for Vacancy Formation Energy – Zr30 at 1200 K

Input file for Vacancy Formation Energy

#---------------INITIALIZATION---------
clear
units   metal
boundary   p p p
atom_style   atomic

#---------------Create Atoms --------------
variable ao equal 3.5325

lattice   bcc 3.5325
region   simbox block -5 5 -5 5 -5 5
create_box   2 simbox
create_atoms   1 region simbox

set   group all type/fraction 2 0.3 7575876

group   zirconium type 2

mass   1 238
mass   2 91
velocity   all create 1200 7273485

#--------------Define Interatomic Potentials--------
pair_style   meam
pair_coeff   * * meamf_uzr1 U Zr meafile_uzr1 U Zr

#-------------Define Settings--------------
compute csym all centro/atom bcc
compute eng all pe/atom
compute eatoms all reduce sum c_eng

#-------------Run Minimization
fix 1 all npt temp 1200.0 1200.0 100.0 iso 0.0 0.0 1000.0
fix 2 all ave/time 1 5000 20000 c_eatoms file averageenergy.txt

```
reset_timestep 0
thermo 1
thermo_style custom step pe lx ly lz press pxx pyy pzz c_eatoms

dump 1 all custom 400 dump.relax.1.* mass type xs ys zs c_csym c_eng

run 20000

run 0
undump 1

#variable N equal count(all), counts the total number of atoms in the cell
#the total number of atoms is stored to the variable N

variable N equal count(all)
variable No equal $N
variable Nzr equal count(zirconium)

#variable Ei equal "c_eatoms" computes the initial energy of the cell system before the vacancy
#E is needed to store the initial energy of the system to the variable Ei

variable E equal "c_eatoms"
variable Ei equal $E


#-------------------------------------------------------
variable r2 equal sqrt(${ao}^2+${ao}^2)/4
#r2 is the radius of the uranium atom

#region select is a region defined so that all atoms within this region are removed
region select sphere 0 0 0 ${r2} units box
delete_atoms region select compress yes
#-------------------------------------------------------
#reset_timestep  0
unfix 1
fix 3 all nvt temp 1200.0 1200.0 100.0
thermo 1
thermo_style custom step pe lx ly lz press pxx pyy pzz c_eatoms

dump 1 all custom 400 dump.relax.2.* mass type xs ys zs c_csym c_eng

run 20000

#variable Ef equal "c_eatoms" computes the final energy of the cell system after the vacancy
#The final energy is stored to the variable Ef

variable Ef equal "c_eatoms"
```

variable Ev equal (${Ef}-((${No}-1)/${No})*${Ei})

Compute zirconium atom fraction

variable frac equal ${Nzr}/${No}

#--

##
SIMULATION DONE
print "All done"
print "Total number of atoms = ${No}"
print "Initial energy of atoms = ${Ei}"
print "Final energy of atoms = ${Ef}"
print "Vacancy formation energy = ${Ev}"
print "Zirconium atom fraction = ${frac}"

Input File for Nearest Neighbors Calculation – Zr30 at 1400 K

Input file for Vacancy Formation Energy

#----------------INITIALIZATION---------
clear
units   metal
boundary   p p p
atom_style   atomic

#----------------Create Atoms --------------
variable ao equal 3.5325

lattice   bcc 3.5325
region   simbox block -5 5 -5 5 -5 5
create_box   2 simbox
create_atoms   1 region simbox

set   group all type/fraction 2 0.3 3065763

variable r2 equal sqrt(${ao}^2+${ao}^2)/4

region one sphere -1.7663 -1.7663 -2.4979 ${r2} units box
set region one type 1
region two sphere 1.7663 -1.7663 -2.4979 ${r2} units box
set region two type 1
region three sphere -1.7663 1.7663 -2.4979 ${r2} units box
set region three type 1

```
region four sphere 1.7663 1.7663 -2.4979 ${r2} units box
set region four type 1
region five sphere -1.7663 -1.7663 2.4979 ${r2} units box
set region five type 2
region six sphere 1.7663 -1.7663 2.4979 ${r2} units box
set region six type 2
region seven sphere -1.7663 1.7663 2.4979 ${r2} units box
set region seven type 2
region eight sphere 1.7663 1.7663 2.4979 ${r2} units box
set region eight type 2


group                   zirconium type 2

mass                    1 238
mass                    2 91
velocity                all create 1400 7289381

#--------------Define Interatomic Potentials--------
pair_style              meam
pair_coeff              * * meamf_uzr1 U Zr meafile_uzr1 U Zr

#-------------Define Settings--------------
compute csym all centro/atom bcc
compute eng all pe/atom
compute eatoms all reduce sum c_eng

#-------------Run Minimization
fix 1 all npt temp 1400.0 1400.0 100.0 iso 0.0 0.0 1000.0
fix 2 all ave/time 1 5000 20000 c_eatoms file averageenergy.txt
reset_timestep 0
thermo 1
thermo_style custom step pe lx ly lz press pxx pyy pzz c_eatoms

dump 1 all custom 400 dump.relax.1.* mass type xs ys zs c_csym c_eng

run 20000

run 0
undump 1

#variable N equal count(all), counts the total number of atoms in the cell
#the total number of atoms is stored to the variable N

variable N equal count(all)
variable No equal $N
variable Nzr equal count(zirconium)
```

```
#variable Ei equal "c_eatoms" computes the initial energy of the cell system before the vacancy
#E is needed to store the initial energy of the system to the variable Ei

variable E equal "c_eatoms"
variable Ei equal $E

#-------------------------------------------------------
#variable r2 equal sqrt(${ao}^2+${ao}^2)/4
#r2 is the radius of the uranium atom

#region select is a region defined so that all atoms within this region are removed
region select sphere 0 0 0 ${r2} units box
delete_atoms region select compress yes
#-------------------------------------------------------
#reset_timestep  0
unfix 1
fix 3 all nvt temp 1400.0 1400.0 100.0
thermo 1
thermo_style custom step pe lx ly lz press pxx pyy pzz c_eatoms

dump 1 all custom 400 dump.relax.2.* mass type xs ys zs c_csym c_eng

run 20000

#variable Ef equal "c_eatoms" computes the final energy of the cell system after the vacancy
#The final energy is stored to the variable Ef

variable Ef equal "c_eatoms"
variable Ev equal (${Ef}-((${No}-1)/${No})*${Ei})

# Compute zirconium atom fraction

variable frac equal ${Nzr}/${No}

#-------------------------------------------------------

####################################################
# SIMULATION DONE
print "All done"
print "Total number of atoms = ${No}"
print "Initial energy of atoms = ${Ei}"
print "Final energy of atoms = ${Ef}"
print "Vacancy formation energy = ${Ev}"
print "Zirconium atom fraction = ${frac}"
```

REFERENCES

Beeler, Benjamin, et al. "First principles calculations of the structure and elastic constants of α, β, and γ uranium." Journal of Nuclear Materials (2012a).

Hofman, G. L., S. L. Hayes, and M. C. Pietri. "Temperature gradient driven constituent redistribution in U-Zr alloys." Journal of Nuclear Materials 227.3 (1996): 277-286.

Hünenberger, Philippe H. "Thermostat algorithms for molecular dynamics simulations." Advanced Computer Simulation. Springer Berlin Heidelberg, 2005. 105-149.

L. C. Walters, B. R. Seidel and J. H. Kittel, Nucl. Technol. 65 (1984) 179.

Mendelev, Mikhail I., and G. J. Auckland. "Development of an interatomic potential for the simulation of phase transformations in zirconium." Philosophical Magazine Letters 87.5 (2007): 349-359.

Mendelev, Mikhail I., and Boris S. Bokstein. "Molecular dynamics study of self-diffusion in Zr." Philosophical Magazine 90.5 (2010): 637-654.

Mendelev, Mikhail I., and Yuri Mishin. "Molecular dynamics study of self-diffusion in bcc Fe." Physical Review B 80.14 (2009).

Moore, Alexander. *Computational Properties of Uranium-Zirconium.* MS Thesis. Georgia Institute of Technology, 2013.

Ogata, Takanari, et al. "Analytical study on deformation and fission gas behavior of metallic fast reactor fuel." Journal of Nuclear Materials 230.2 (1996): 129-139.

Ogata, Takanari, et al. "Reactions between U-Zr alloys and Fe at 923 K." Journal of Nuclear Materials 250.2 (1997): 171-175.

Okamoto, H. (2007). "U-Zr (Uranium-Zirconium)." Journal of Phase Equilibria and Diffusion 28(5): 499-500.

Ondracek, Gerhard, and Brigitte Shulz. "The porosity dependence of the thermal conductivity for nuclear fuels." Journal of Nuclear Materials 46.3 (1973): 253-258.

Pahl, Porter, Crawford and Walters. Irradiation behaviors of metallic fast reactor fuels, Journal of Nuclear Materials 188 (1992) 3-9.

Pahl, R.G., et al. "Experimental studies of U-Pu-Zr fast reactor fuel pins in the experimental breeder reactor-II." Metallurgical Transactions A 21.7 (1990): 1863-1870.

Steven L. Hayes and Douglas L. Porter, Fast Reactor Fuels, Nuclear Fuels and Materials Division Fuel Performance and Design Department, June 5, 2009.

W. M. Stacey, et al., "Resolution of Fission and Fusion Technology Integration Issues: An Upgraded Design Concept for the Subcritical Advanced Burner Reactor (SABR)", Nuclear Technology (to be published).

Y. S. Kim, G. L. Hofman, S. L. Hayes, Y. H. Sohn, J. Nuc. Mat. 327 (2004) 27-36.